University of Massachusetts Medical School

eScholarship@UMMS

University of Massachusetts Medical School Faculty Publications

2020-12-20

Linker histone H1.8 inhibits chromatin-binding of condensins and DNA topoisomerase II to tune chromosome compaction and individualization [preprint]

Pavan Choppakatla
Rockefeller University

Et al.

Let us know how access to this document benefits you.

Follow this and additional works at: https://escholarship.umassmed.edu/faculty_pubs

Part of the Amino Acids, Peptides, and Proteins Commons, Cell Biology Commons, Molecular Biology Commons, Structural Biology Commons, and the Systems Biology Commons

Linker histone H1.8 inhibits chromatin-binding of condensins and DNA topoisomerase II to tune chromosome compaction and individualization

Pavan Choppakatla[1], Bastiaan Dekker[2], Erin E. Cutts[3], Alessandro Vannini[3,4], Job Dekker[2, 5]and Hironori Funabiki[1, *]

[1]Laboratory of Chromosome and Cell Biology, The Rockefeller University, New York, NY 10065, USA.

[2]Program in Systems Biology, Department of Biochemistry and Molecular Pharmacology, University of Massachusetts Medical School, Worcester, MA 01605, USA.

[3]Division of Structural Biology, The Institute of Cancer Research, London SW7 3RP, UK.

[4]Fondazione Human Technopole, Structural Biology Research Centre, 20157 Milan, Italy

[5]Howard Hughes Medical Institute, Chevy Chase, MD 20815, USA.

*Correspondence: funabih@rockefeller.edu

Summary

DNA loop extrusion by condensins and decatenation by DNA topoisomerase II (topo II) drive mitotic chromosome compaction and individualization. Here, we reveal that the linker histone H1.8 regulates chromatin levels of condensins and topo II. *In vitro* chromatin reconstitution experiments demonstrate that H1.8 inhibits binding of condensins and topo II to nucleosome arrays. Accordingly, H1.8 depletion in *Xenopus* egg extracts increased condensins and topo II levels on mitotic chromatin. Chromosome morphology and Hi-C analyses suggest that H1.8 depletion makes chromosomes thinner and longer likely through shortening the average loop size and reducing DNA amount in each layer of mitotic loops. Furthermore, H1.8-mediated suppression of condensins and topo II binding to chromatin limits chromosome individualization by preventing resolution of interchromosomal linkages. While linker histones locally compact DNA by clustering nucleosomes, we propose that H1.8 controls chromosome morphology and topological organization through restricting the loading of condensins and topo II on chromatin.

Keywords

Chromosome compaction, chromatin, mitosis, linker histone, nucleosome, condensin, DNA topoisomerase, Hi-C, Xenopus

---

Introduction

Genomic DNA in eukaryotes is compacted by orders of magnitude over its linear length. The extent and mode of the packaging change between interphase and mitosis to support the cell cycle dependent functions of the DNA. While loosely packed DNA allows efficient decoding of genetic information in interphase, mitotic compaction of DNA enables efficient distribution of genetic information to daughter cells. In addition, chromosome individualization during mitosis ensures that all duplicated chromosomes are independently moved by microtubules and are equally distributed to daughter cells. Despite these common functional requirements of mitotic chromosomes and

evolutionary conservation of major known regulators of mitotic chromosome structures, the size and shape of chromosomes vary widely among species and developmental stages. For example, rod-like individual chromosomes can be readily visualized in fission yeast *Schizosaccharomyces pombe*, but not in budding yeast *Saccharomyces cerevisiae* (Guacci et al., 1994; Umesono et al., 1983). During early embryogenesis in *Xenopus* and *C. elegans*, chromosome lengths become shorter (Ladouceur et al., 2015; Micheli et al., 1993). The mechanistic basis of mitotic chromosome shape regulation remains largely speculative (Heald and Gibeaux, 2018).

Classical experiments on mitotic chromosomes indicated that DNA is organized into loops around a central protein scaffold (Earnshaw and Laemmli, 1983; Paulson and Laemmli, 1977). Two major chromosome-associated ATPases play pivotal roles in mitotic chromatid formation: the DNA topoisomerase II (topo II) and the structural maintenance of chromosomes (SMC) family complex, condensin. Data obtained with chromosome conformation capture assays are consistent with the model that mitotic chromosomes are arranged in a series of loops organized by condensins (Gibcus et al., 2018; Naumova et al., 2013). Vertebrate cells express two forms of the condensin complex, condensin I and condensin II (Ono et al. 2003). Condensin I is loaded onto chromatin exclusively during mitosis, whereas condensin II retains access to chromosomes throughout the cell cycle (Hirota et al. 2004; Walther et al. 2018). Condensin II plays a role in maintaining chromosome territories in *Drosophila* nuclei (Rosin et al., 2018) and drives sister chromatid decatenation by topo II (Nagasaka et al., 2016). It has been proposed that condensin II anchors large outer DNA loops, which are further branched into shorter inner DNA loops by condensin I (Gibcus et al., 2018). This proposal is consistent with their localization determined by super-resolution microscopy (Walther et al., 2018). In chicken DT40 cells, condensin II drives the helical positioning of loops around a centrally located axis thus controls the organization of long distance interactions (6- 20 Mb), whereas condensin I appears to control shorter distance interactions (Gibcus et al., 2018). In *Xenopus* egg extracts, condensin I, which is five-fold more abundant than condensin II, plays a larger role than condensin II in regulating mitotic chromosome length (Ono et al., 2003; Shintomi and Hirano, 2011).

The prevailing model suggests that mitotic chromatin loops are formed by the dynamic loop extrusion activity of condensins (Alipour and Marko, 2012; Nasmyth, 2001; Riggs, 1990), although the molecular details of the process remain unclear (Banigan and Mirny, 2020; Cutts and Vannini, 2020; Datta et al., 2020). Single molecule experiments using purified recombinant yeast and human condensin complexes demonstrated ATP-dependent motor activity and loop extrusion by yeast and human condensins (Ganji et al., 2018; Kong et al., 2020; Terakawa et al., 2017). Condensin dependent loop extrusion in a more physiological *Xenopus* extract system has also been shown (Golfier et al., 2020). *In silico* experiments suggest that a minimal combination of loop extruders (like condensin) and strand passage activity (such as topo II) can generate well resolved rod-like sister chromatids from entangled, interphase like DNA fibers (Goloborodko et al., 2016a).

These demonstrations of loop extrusion by purified condensins and cohesin were all largely performed on naked DNA substrates. However, loops that comprise metazoan mitotic chromosomes contain 100-200 kb of DNA (Banigan and Mirny, 2020), which represents hundreds of nucleosomes. Since condensins prefer to bind non-nucleosomal DNA (Kong et al., 2020; Shintomi et al., 2017; Zierhut et al., 2014), it remains unknown if loop extrusion can proceed on chromatin. Human condensin complexes appear to be capable of loop extrusion through sparsely arranged nucleosomes (Kong et al., 2020). However, mitotic chromatin also appears to adopt a more compact fiber structure (Grigoryev et al., 2016), and large protein complexes such as RNA polymerases are able to limit loop extrusion by SMC protein complexes, such as bacterial condensins and eukaryotic cohesins (Brandão et al., 2019; Hsieh et al., 2020; Krietenstein et al., 2020). Therefore, the effect of higher order chromatin fiber structure and other mitotic chromatin proteins on processive loop extrusion by condensin remains unknown.

Interphase nuclei are composed of largely separated chromosome territories and highly entangled sister chromatids after replication (Cremer and Cremer, 2010; Farcas et al., 2011; Sundin and Varshavsky, 1981). Replicated pairs of chromatids are linked by cohesin during interphase, and cohesin removal during prophase (except at centromeres and a limited number of chromosome loci along chromosome arms) promotes resolution of sister chromatids, together with actions of condensin II and topo II (Nagasaka et al., 2016). Different chromosomes are also largely unentangled in

interphase HeLa cells (Goundaroulis et al., 2020; Tavares-Cadete et al., 2020), and Ki-67 localization on chromosome peripheries may act as a steric and electrostatic barrier to prevent interchromosomal entanglement during mitosis (Cuylen et al., 2016), but some interchromosomal linkages remain in metaphase (Marko, 2008; Potapova et al., 2019). Although increased transcription and topo II activity seem to be involved in the generation and resolution of some interchromosomal links (Potapova et al., 2019), the abundance and significance of these and other interchromosomal entanglements is still unknown.

One of the most abundant chromatin proteins beside core histones is the linker histone, which binds to the dyad of the nucleosome and tethers the two linker DNAs emanating from the nucleosome (Bednar et al., 2017). In reconstitution experiments, linker histones cluster oligo- nucleosomes (Li et al., 2016; White et al., 2016), and promote liquid-liquid phase separation (Gibson et al., 2019; Shakya et al., 2020). *In vivo,* linker histones are also enriched in highly compact chromatin (Izzo et al., 2013; Parseghian et al., 2001; Th'ng et al., 2005). While core histones are evolutionarily highly conserved in eukaryotes, linker histones are much more diversified (Hergeth and Schneider, 2015; Izzo et al., 2008). In the human and mouse genome, 11 H1 paralogs are found, among which five (H1.1-H1.5) are widely expressed in somatic cells. In vertebrate oocytes and early embryos, a tissue specific linker histone variant H1.8 (also known as H1OO, H1foo, H1M and B4) is the major linker histone variant (Dworkin-Rastl et al., 1994; Wühr et al., 2014). Immuno-depletion of H1.8 from *Xenopus* egg extracts made mitotic chromosomes thinner and longer, causing defective chromosome segregation in anaphase (Maresca et al., 2005). However, the mechanism by which the linker histone affects large scale chromosome length changes remains unknown.

Here we demonstrate that the linker histone H1.8 suppresses enrichment of condensins and topo II on mitotic chromosomes. In a reconstitution system with purified components, H1.8 inhibits binding of topo II and condensins to nucleosome arrays. Through a combination of chromosome morphological analysis and Hi-C, we show that H1.8 reduces chromosome length by limiting condensin I loading on chromosomes, while H1.8 limits chromosome individualization by reducing the loading of both condensins and suppressing topo II. This study establishes a mechanism by which the linker histone tunes the compaction and topology of mitotic chromosomes.

Results

Linker histone H1.8 limits enrichment of condensins and topo II on mitotic chromatin

Depletion of linker histone H1.8 in *Xenopus* egg extracts makes chromosomes thinner and elongated (see **Figure 3C;** Maresca et al., 2005). We asked if this phenotype may reflect the potential role of H1.8 in regulating condensins and TOP2A (the dominant topo II isoform in *Xenopus* egg extracts, Wühr et al., 2014), which are essential for mitotic chromosome compaction in *Xenopus* egg extracts (Adachi et al., 1991; Cuvier and Hirano, 2003; Hirano and Mitchison, 1994). *In silico* simulation analysis suggests that increasing the number of loop extruders (such as condensin I) on DNA makes chromosomes longer and thinner (Goloborodko et al., 2016a). Reducing condensin I levels on chromatin also made chromosomes shorter in *Xenopus* egg extracts (Shintomi and Hirano, 2011). Although it has been reported that H1.8 depletion does not affect enrichment of major chromatin proteins (Maresca et al., 2005), we therefore attempted to quantify chromatin-bound amounts of condensins and TOP2A.

To investigate whether H1.8 regulates chromatin levels of condensins and topo II, we prepared mitotic chromosomes in *Xenopus laevis* egg extracts depleted of H1.8. Demembranated *Xenopus laevis* sperm nuclei were added to either mock (ΔIgG) or H1.8 depleted (ΔH1) extracts from eggs arrested at meiotic metaphase II by cytostatic factor (CSF extracts) (**Figure 1B**). Calcium was added to cycle the extract into interphase and induce replication of sperm chromosomes. After replication was finished, mitosis was induced by adding the corresponding depleted CSF extract to generate metaphase chromosomes (**Figure 1A**). To eliminate the microtubule-dependent change in chromosome morphology, which may affect quantitative analyses of chromatin proteins, spindle assembly was inhibited using nocodazole. Chromosomes were fixed and the levels of TOP2A and condensin I subunit xCAP-G were measured by immunofluorescence (**Figure 1C**). Depletion of H1.8 increased the levels of both xCAP-G and TOP2A on mitotic chromosomes, while adding back recombinant H1.8 rescued the phenotype (**Figure 1D**). Identical results were obtained when immunofluorescence signal normalization was done

Choppakatla et al., Dec 2020-preprint copy- BioRxiv
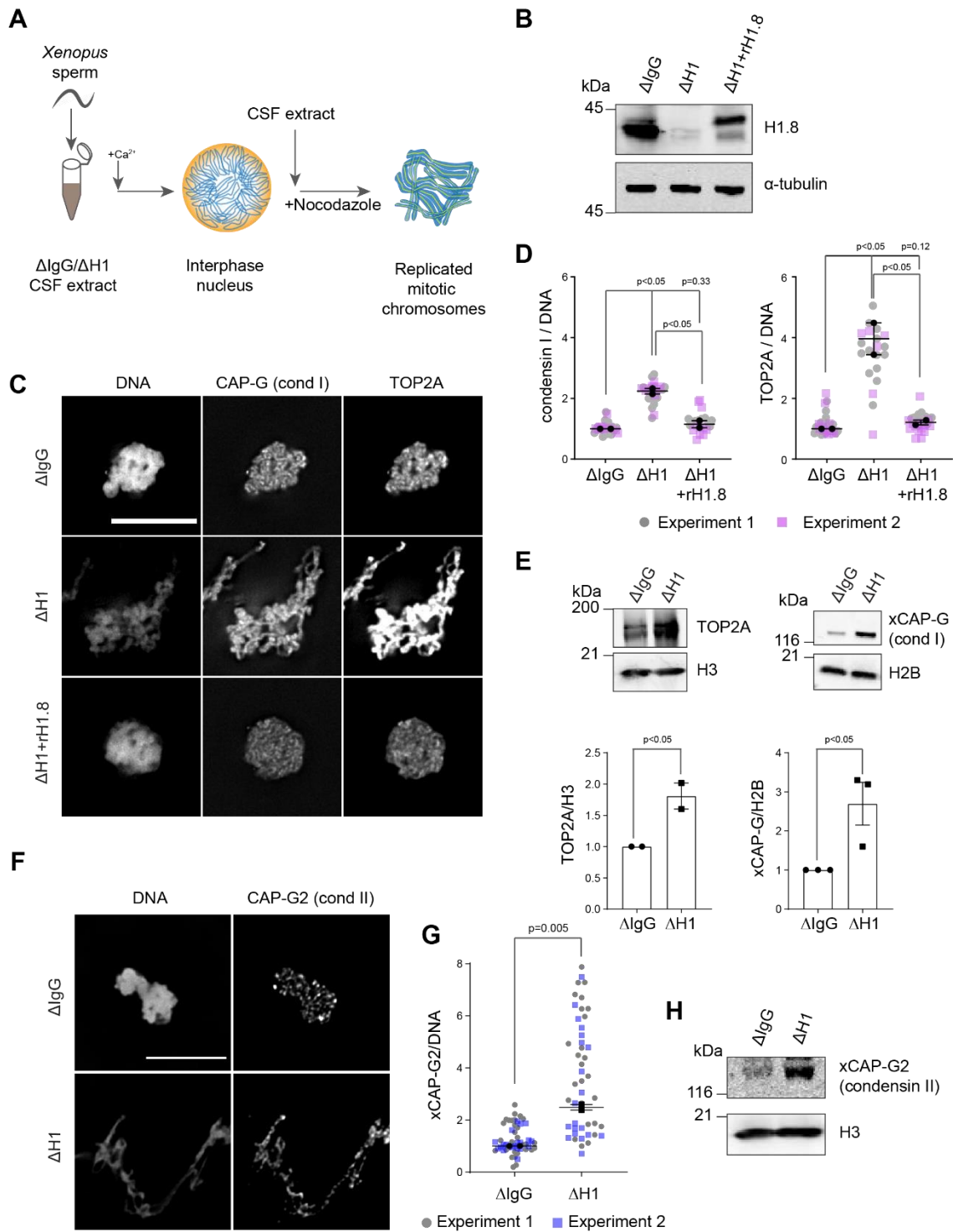
Figure 1. **Linker histone H1.8 suppresses enrichment of condensins and TOP2A on mitotic chromatin**

A) Experimental scheme to generate replicated chromosomes in *Xenopus* egg extracts. B) Western blots showing depletion of H1.8 from *Xenopus* egg extracts and rescue with recombinant H1.8 (rH1.8). C) Representative images of DNA (Hoechst 33342), CAP-G (condensin I) and TOP2A immunofluorescence on chromosomes in metaphase extracts treated with nocodazole in the indicated conditions. Chromosomes in each nucleus remain clustered in the presence of nocodazole. Bar, 10 µm. D) Quantification of CAP-G (condensin I) and TOP2A immunofluorescence signals normalized to the DNA (Hoechst) signal for the indicated conditions. Each grey or magenta dot represents the average signal intensity of a single chromosome cluster (from one nucleus). Each black dot represents the median signal intensity from a single experiment. Bars represent mean and range of the medians of two independent experiments. For each experiment, signals on >20 chromosome clusters were counted. E) Western blots of mitotic chromatin purified from mock (ΔIgG) and H1.8-depleted (ΔH1) extracts (top) and quantification of band intensities normalized to H3 and H2B (below). Mean and SEM from 3 experiments. F) Representative images of CAP-G2 (condensin II) immunofluorescence on chromosomes in metaphase extracts with nocodazole in the indicated conditions. Bar, 10 µm. G) Quantification of the CAP-G2 (condensin II) normalized to the DNA (Hoechst) signal for the indicated conditions. Each grey or purple dot represents the average signal intensity of a single chromosome cluster (from one nucleus). Each black dot represents the median signal intensity from a single experiment. Bars represent mean and range of the median of two independent experiments. For each experiment, signals on >20 chromosome clusters were counted. H) Western blots of mitotic chromatin purified from mock (ΔIgG) and H1.8-depleted (ΔH1) extracts.

by Hoechst 33342, or by fluorescent dUTP that was incorporated during replication (**Figure S1A, B**). The dUTP quantitation also confirmed that H1.8 depletion did not affect DNA replication. The apparent increased signals of xCAP-G and TOP2A on chromatin in ΔH1 extracts were not the general consequence of elongated chromosome morphology, since signal intensities of a panel of other proteins did not show similar increases due to H1 depletion, regardless of their preference of nucleosomes or nucleosome-free DNA (Zierhut et al., 2014) (**Figure S1D**). Enhanced chromosome binding of condensin I and TOP2A in ΔH1.8 extracts was biochemically confirmed by quantifying their levels on purified metaphase chromosomes by western blotting (**Figure 1E**). Condensin II levels on chromosomes also showed similar increases in ΔH1 extracts (**Figure 1F, G, H**).

Linker histone H1.8 reduces binding of condensins and TOP2A to nucleosome arrays

Since linker histone depletion does not change the nucleosome spacing in *Xenopus* egg extracts (Ohsumi, Katagiri, & Kishimoto, 1993), we hypothesized that H1.8 depletion results in an increase in free linker DNA that becomes accessible to condensins and TOP2A. To test this possibility, we reconstituted nucleosome arrays with purified histones, and asked if H1.8 interferes with binding of recombinant human condensins and *X. laevis* TOP2A (Kong et al., 2020) (**Figure 2A**). The nucleosome array was composed of 19 tandem repeats of 147 bp Widom nucleosome positioning sequence and 53 bp linker DNA (Lowary and Widom, 1998), where full occupancy of the array by nucleosome core particle (NCP) and H1.8 to each repeat unit was confirmed by native polyacrylamide gel electrophoresis (PAGE) (**Figure S2A**).

The recombinant human condensin I, but not the ATP-binding defective Q-loop mutant (Hassler et al., 2019; Hopfner et al., 2000; Kong et al., 2020; Löwe et al., 2001), was able to rescue chromatid formation in condensin I depleted *Xenopus* extracts (**Figure S2B**), demonstrating that the recombinant human condensin I can functionally replace *Xenopus* condensin I. As reported previously (Kong et al., 2020), condensin I bound weakly to nucleosomes with linker DNA, and this weak binding was stimulated by ATP (**Figure S2C**). Surprisingly, both wild-type and the Q-loop mutant of condensin I showed similar ATP-dependent enhancement of binding to the nucleosome array, while this

enhancement was not seen when magnesium concentration was higher than the ATP concentration (**Figure S2D**). This suggests that ATP promotes condensin binding to nucleosomes independent of ATP-binding capacity of condensin I. Both EDTA and ATP, which chelate magnesium, increased binding of the Q loop mutant of condensin I to the nucleosome array (**Figure S2E**), suggesting that condensin binding to the nucleosome array is sensitive to high magnesium concentration, which is known to induce chromatin compaction (Eltsov et al., 2008; Finch and Klug, 1976).
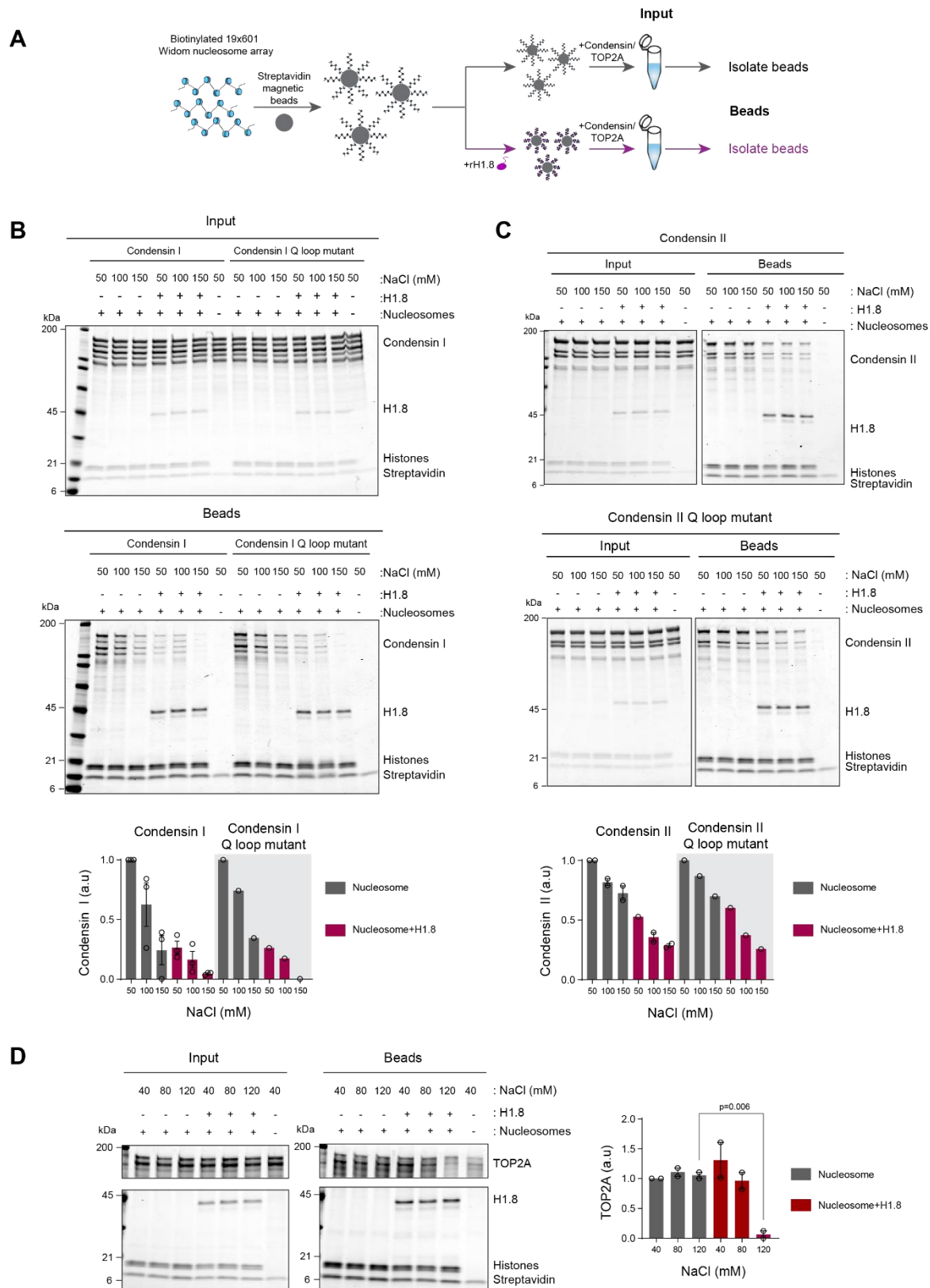
In the buffer condition where excess ATP was present over magnesium, both wild-type and the Q-loop mutant of condensin I showed reduced binding to nucleosome arrays loaded with H1.8 at physiological salt concentrations (50 – 150 mM NaCl) (**Figure 2B**). H1.8 also suppressed binding of Condensin II and its Q-loop mutant to the nucleosome array (**Figure 2C**), though, as expected (Kong et al., 2020), condensin II showed higher affinity to the nucleosome array than condensin I. This reduced binding of condensins in the presence of H1.8 can be explained by either direct competition between H1.8 and condensins for the linker DNA or by H1.8-mediated formation of a higher order structure of the nucleosome array (Song et al., 2014). To distinguish between these two possibilities, we asked if H1.8 inhibits condensin I binding to mononucleosomes, since H1.8 binding to mononucleosomes does not promote higher order structure or aggregation (**Figure S2F**). Consistent with the direct competition model, H1 reduced binding of condensin I to mononucleosomes (**Figure S2F**).

We also performed similar experiments with recombinant *X. laevis* TOP2A purified from yeast (**Figure S2G, S2H**). TOP2A shows more stable binding to chromatin, and H1.8 has no effect on TOP2A binding at low salt concentrations. However, H1.8 did reduce nucleosome array binding of recombinant *X. laevis* TOP2A at 120 mM NaCl (**Figure 2D**). Altogether, these data demonstrate that preloaded H1.8 on nucleosomes can directly interfere with binding of condensins and TOP2A to chromatin.

Chromosome elongation by H1.8 depletion is due to increased chromatin bound condensin I

If the increased amount of condensin I on chromatin is responsible for the chromosome elongation phenotype observed in ΔH1 extracts, we expect that reducing condensin I levels should rescue this

Choppakatla et al., Dec 2020-preprint copy- BioRxiv

Figure 2. Linker histone inhibits binding of condensins and TOP2A to nucleosome arrays

A) Experimental scheme for testing the effect of recombinant H1.8 (rH1.8) on binding of purified condensins and TOP2A to arrays of nucleosomes assembled on the Widom 601 nucleosome positioning sequence. B) Coomassie staining of SDS-PAGE gels, showing input (top) and nucleosome-array bound fraction (middle) of condensin I, rH1.8 and core histones. The right most lanes represent the streptavidin beads only negative control. Buffer contains 2.5 mM $MgCl_2$, 5 mM ATP and indicated concentrations of NaCl. The band intensities of condensin I subunits were normalized to the histone bands and the binding at 50 mM NaCl for nucleosome arrays without H1.8. Mean and S.E.M of three independent experiments are shown (bottom). C) Same as B, except that nucleosome array binding of condensin II is shown. Mean and range of two independent experiments are shown. D) Same as B, except that nucleosome array binding of TOP2A in buffer containing 1 mM $MgCl_2$ is shown. Mean and range of two independent experiments are shown.

phenotype. Since chromosomes from a nucleus remain clustered in crude metaphase egg extracts, we diluted metaphase extracts before fixation to disperse individual chromosomes (**Figure 3A, 3B**) (Funabiki and Murray, 2000). This enabled measurement of chromosome length. Average chromosome length increased by ~50% in ΔH1 extracts, as reported previously (Maresca et al., 2005). Consistent with our hypothesis, when condensin I was co-depleted (ΔH1ΔCAP-G), chromosomes became shorter than chromosomes in mock depleted extracts (ΔIgG)

(**Figure 3C, 3D**). In contrast, condensin II co-depletion (ΔH1ΔCAP-D3) did not change the chromosome length (**Figure 3D**). Chromosome length in condensin II-depleted extracts (ΔCAP-D3) is also indistinguishable from mock depleted chromosomes (**Figure S3A**), consistent with the reduced role of condensin II in the presence of wild-type condensin I levels (Shintomi and Hirano, 2011). These data support the idea that chromosome elongation upon H1.8 depletion is caused by increased levels of condensin I on chromosomes.
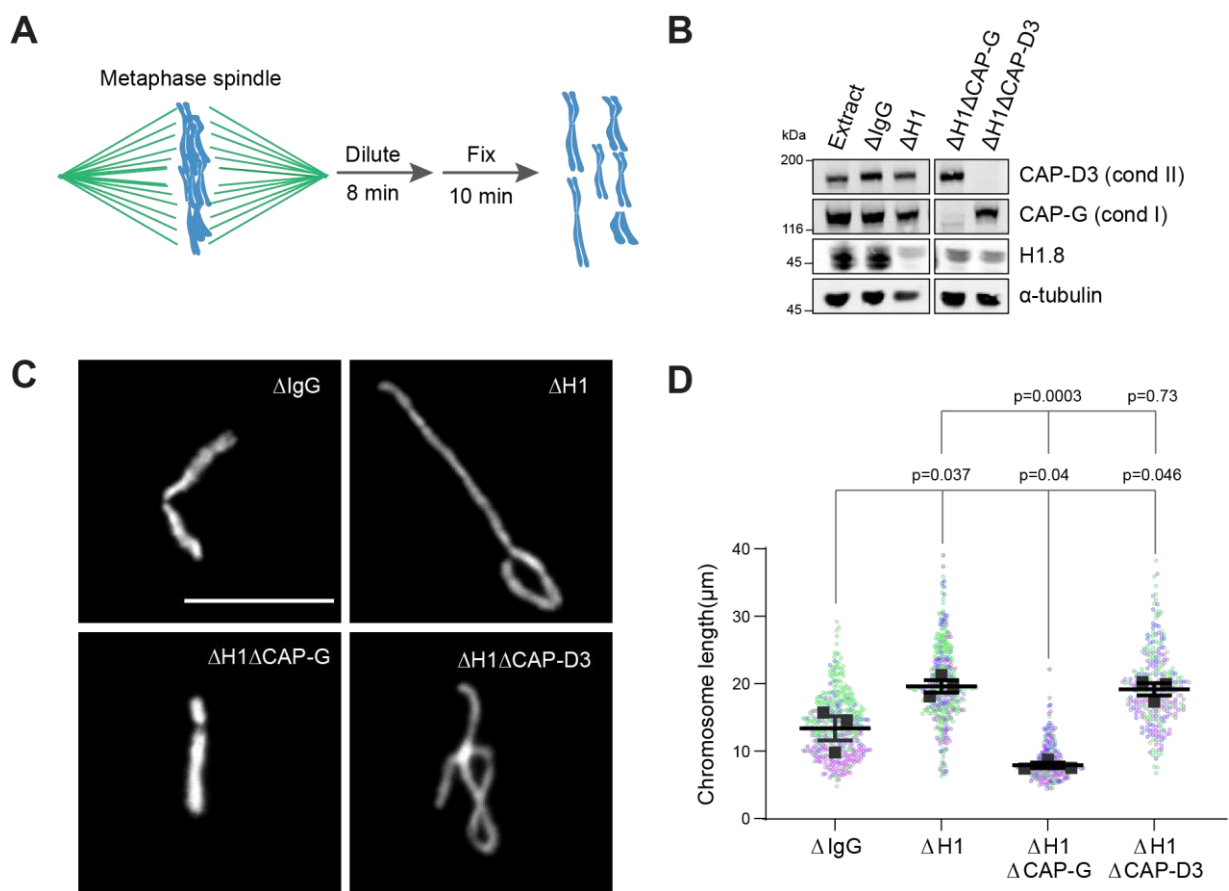
Figure 3. Chromosome elongation by H1.8 depletion is due to enhanced condensin I loading on chromatin

A) Schematic of extract dilution to disperse individualized chromosomes. B) Western blots of egg extracts showing depletions of indicated proteins. C) Representative images of mitotic chromosomes after dilution of indicated extracts. Bar, 10 μm. D) Quantification of the chromosome length. Data distribution of the length of individual chromosomes from three independent experiments (green, purple, grey) is shown. Each black dot represents the median length of chromosomes from a single experiment. Bar represents mean and S.E.M of three independent experiments. The length of >50 chromosomes were measured in each condition for every experiment.

H1.8 increases condensin I driven mitotic loop layer organization

The level of condensin I association with chromosomes is proposed to regulate chromosome length through changing loop size (Gibcus et al., 2018; Goloborodko et al., 2016b, 2016a). Low levels

of condensin I is predicted to result in fewer and larger loops, while higher levels of condensin I binding will lead to smaller but more numerous loops. Therefore, if linker histone H1.8 decreases chromosome length through limiting condensin I association with chromatin, we expect that the average size of mitotic loops decreases upon H1.8

depletion. To estimate the loop size and investigate other structural effects of H1.8 depletion, we used the chromosome conformation capture assay Hi-C (Lieberman-Aiden et al., 2009) on metaphase sperm chromosome samples prepared from *Xenopus* egg extracts.

Hi-C contact probability maps were generated from replicated metaphase chromosomes 60 min after cycling back into mitosis in the presence of nocodazole. As reported previously (Gibcus et al., 2018; Naumova et al., 2013), all the Hi-C contact maps showed no checkerboard pattern commonly associated with interphase chromosome compartments, and lacked any sign of topologically associating domains (TADs) (Szabo et al., 2019) (**Figure 4A**). Hi-C interaction maps are characterized by the decay in contact probability (P) with genomic distance (s). To derive quantitative information about the polymer structure of the mitotic chromosomes, we plotted the genome-wide average $P(s)$ (**Figure 4B**). $P(s)$ plots are consistent among two biological replicates (**Figure S4A**) and among each individual chromosome (**Figure S4B**). The interaction decay profile of the control (ΔIgG) chromosomes are also qualitatively similar to mitotic chromosomes in both DT40 and HeLa cells (Gibcus et al., 2018; Naumova et al., 2013). Consistent with the major role of condensin I in mitotic chromosome organization, condensin I depletion (ΔCAP-G) caused a major change in the Hi-C map (Figure 4A), though unlike in DT40 cells, condensin I depletion affected interactions at longer distances (~ 10 Mb), whereas condensin II depletion (ΔCAP-D3) did not cause recognizable changes in interactions at both long and short distances (**Figure S4C**). A second diagonal band, which is indicative of a strong helical organization in the chromosome axis (Gibcus et al., 2018), was not seen in *Xenopus* egg extracts (**Figure 4A, S4C**), likely reflecting the minor contribution of condensin II in this system and also a prolonged arrest in mitosis (Gibcus et al., 2018). In H1.8-depleted extracts (ΔH1), a dramatic decrease in interactions at long genomic distances (1-10 Mb) was observed (**Figure 4A, 4B**), as expected from their thinner chromosome morphology (**Figure 3**).

$P(s)$ plots are useful to determine the underlying polymer structure of the chromosome such as average loop size (Gibcus et al., 2018). Specifically, the first derivative of the $P(s)$ plots can reveal both the average loop size and the amount of DNA per layer of the rod-shaped mitotic chromosome (layer size) (Abramo et al., 2019; Gassler et al., 2017; Gibcus et al., 2018) (**Figure 4C**).

Average loop size can be estimated from the peak value in the derivative plot (Gassler et al., 2017; Patel et al., 2019). As the derivative plot in our data showed a peak in the 10 kb-1 Mb range, we estimated that this peak location reflects the average loop size. Unlike mitotic chromosomes in DT40 or HeLa cell lines (Abramo et al., 2019; Gibcus et al., 2018), metaphase chromosomes from *Xenopus* extracts have a flattened peak (**Figure 4C**), possibly due to a larger variation in loop sizes. Although it is difficult to estimate the exact loop size from these plots, chromosomes from ΔH1 extracts show a reproducible shift of the peak towards smaller genomic distances (**Figure 4C**). This is consistent with a decrease in loop size due to increased condensin I accumulation on chromatin upon H1.8 depletion. Derivative plots generated from Hi-C maps of dispersed chromosomes (**Figure 3A**) from both control (ΔIgG) and H1.8 depleted extracts (ΔH1) show similar shift in peak towards smaller genomic distances upon H1.8 depletion (**Figure S4D**). The derivative plots from dispersed chromosomes show a better-defined peak, allowing a more precise loop size estimate of 140 kb in ΔIgG extracts and 110 kb in ΔH1 extracts. These loop sizes are comparable to the size of condensin I-driven loops in DT40 and HeLa cells (Gibcus et al., 2018; Naumova et al., 2013).

$P(s)$ plots for mitotic chromosomes display three regimes that are typical for relatively stiff rod-shaped conformation (Gibcus et al., 2018; Naumova et al., 2013): for small genomic distance the contact probability is dominated by interactions between pairs of loci located within loops (up to 1-200 kb). For loci separated by up to a few megabases, the contact probability decays slowly with genomic distance and for this distance range interactions mostly reflect contacts between loci located in different loops but these loops are relatively closely packed as a radial layer of loops around the central axis (intra-layer regime). The third regime is characterized by a steep decay in contact probability at several megabases. This represents pairs of loci separated by a relatively large distance along the axis of the rod-shaped chromosome so that they very rarely interact (inter-layer regime). The size of these layers can be obtained from the derivative of $P(s)$, where the steep drop in contact probability curve is marked by sharp drop in the derivative value. For control chromosomes the average amount of DNA in each layer of loops (layer size) is approximately 5 Mb, given the steep decay in contact probability observed for loci separated by more than 5 Mb for

Choppakatla et al., Dec 2020-preprint copy- BioRxiv
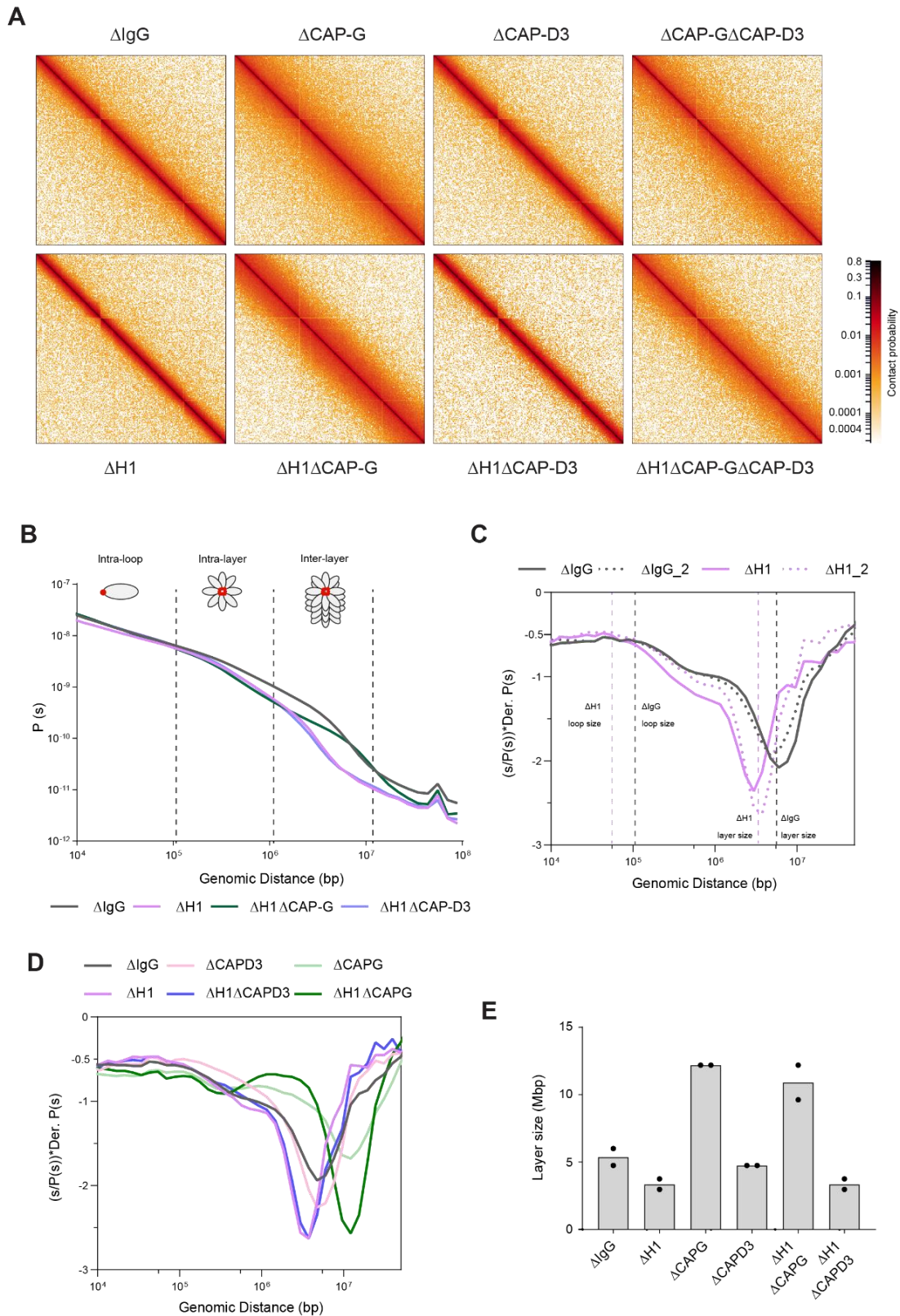
Figure 4. Effects of H1 and/or condensin I, II depletion on mitotic genome folding

A) Genome averaged Hi-C maps of metaphase *X. laevis* chromosomes in the indicated condition. B) Genome wide average contact probability decay curves for the indicated conditions showing the changes in longer distance interactions. C) Derivative plots of the average contact probability decay curves for mock (ΔIgG) and H1.8 depleted extracts (ΔH1) showing the change in estimated loop size and indicating amount of DNA per layer. The solid and dotted lines are from two independent biological replicates.D) Derivative plots of the genome wide average contact probability decay curves in the indicated conditions.E) Estimates of DNA per layer from derivatives of genome wide probability decay curves upon depletion of H1.8 and CAP-G (condensin I) or CAP-D3 (condensin II). Mean and range of two independent experiments are shown.

both replicates (**Figure 4B, 4C**). For H1.8 depleted chromosomes we observe a smaller layer size of around 3.5 Mb (**Figure 4B, 4C**). This 1.5-fold reduction of DNA content of each layer would explain the observed 1.5-fold increase in chromosome length (**Figure 3B**). Further, we can derive the number of loops per layer by dividing the layer size by the loop size in the corresponding condition. In both control (ΔIgG) and H1.8 depleted extracts (ΔH1), the number of loops per layer is ~40. This indicates that the change in the layer size upon H1.8 depletion is a result of decreased loop size, while the number of loops per layer is not affected.

The layer size in H1.8/condensin I co-depleted extracts (ΔH1ΔCAP-G) is larger than those in control extracts (ΔIgG) (**Figure 4D, E**). This is consistent with the shorter chromosomes in ΔH1ΔCAP-G extracts than in control ΔIgG extracts (**Figure 3**). Condensin II co-depletion (ΔH1ΔCAP-D3) did not affect the layer size (3.5 Mb) and also the chromosome length (**Figure 4D, 4E, 3D**). Condensin II depletion alone (ΔCAP-D3) also did not affect the layer size, consistent with the observed lack of change in the chromosome length (**Figure 4D, 4E, S3A**). Taken together, these data support the hypothesis that H1.8 limits the condensin I level on chromatin and shortens chromosome lengths, allowing each condensin I to form a longer loop, and consequentially tuning the amount of DNA present in each layer. The data also suggest that unlike in chicken DT 40 cells, condensin I plays the dominant role in the organization of loop layers (Gibcus et al., 2018).

Since condensin I binding to DNA is also limited by nucleosomes (Kong et al., 2020; Shintomi et al., 2017; Zierhut et al., 2014), we expected that loss of nucleosomes would similarly reduce the loop and layer sizes. To test this, we depleted H3-H4 tetramers using an antibody to acetylated lysine 12 of histone H4 (H4K12ac)(Zierhut et al., 2014), and generated metaphase chromosomes for Hi-C (**Figure S4E**). Since *X. laevis* sperm contains preloaded paternal H3-H4 (Shechter et al., 2009), the number of nucleosomes in our metaphase chromosomes was expected to be reduced by at most 50 %. Histone depletion (ΔH3-H4) increased chromatin bound condensin I beyond that of H1.8 depletion (ΔH1) (**Figure S4F**). Consequentially, the layer size in ΔH3-H4 extracts became much smaller (around 500 kb) than in ΔH1 extracts (**Figure S4G**). Assuming that the number of loops per layer is similar in these chromosomes (~40), the loop size estimate is 12 kb, which is much shorter than in H1.8 depletion.

Altogether these results suggest that global occupancy of nucleosomes and linker histones can affect DNA loop size and chromosome through controlling the number of condensin molecules on the chromatin fiber.

H1.8 suppresses condensin-driven mitotic chromosome individualization.

Condensins and topo II act in concert to generate mitotic chromosomes from decondensed interphase nuclei (Cuvier and Hirano, 2003). Both experimental observations and *in silico* experiments also suggest that condensin is required to complete decatenation of sister-chromatids (Goloborodko et al., 2016a; Nagasaka et al., 2016). Condensin is also required to keep decatenating sister chromatids in metaphase (Piskadlo et al., 2017). Although it has been suggested that condensin-mediated chromosome compaction promotes chromosome individualization (Brahmachari and Marko, 2019; Sun et al., 2018), it remains to be established if different linear chromosomes (non-sisters) are catenated with each other even after completion of mitotic compaction since Ki-67 on chromosome surface may act as a barrier to prevent interchromosomal DNA interaction during mitosis (Cuylen et al., 2016). To investigate if substantial interchromosomal entanglements exist in metaphase *Xenopus* egg extracts, we examined if topo II inhibitor ICRF-193 blocks chromosome individualization after mitotic chromosome compaction (**Figure S5A**). While chromosomes clustered on the metaphase spindle in DMSO-treated control extracts were effectively dispersed into individualized chromosomes after diluting extracts, most chromosomes remained clustered when ICRF-193 was added at the beginning of mitotic induction and incubated for 50 min (**Figure S5B, C, ICRF-50 min**). Even when ICRF-193 was added to metaphase egg extracts after completion of metaphase spindle formation but 2 min before extract dilution (**Figure S5A**, bottom), efficiency of chromosome individualization decreased (**Figure S5B, C**, ICRF-2 min). These results suggest that substantial interchromosomal topological catenations remain unresolved in metaphase.

We then asked if H1.8-mediated suppression of condensins limits chromosome individualization. If so, H1.8 depletion may reduce the minimum required level of condensin activities to support chromosome individualization. In metaphase mock-depleted (ΔIgG) and H1.8-depleted (ΔH1) extracts

Choppakatla et al., Dec 2020-preprint copy- BioRxiv
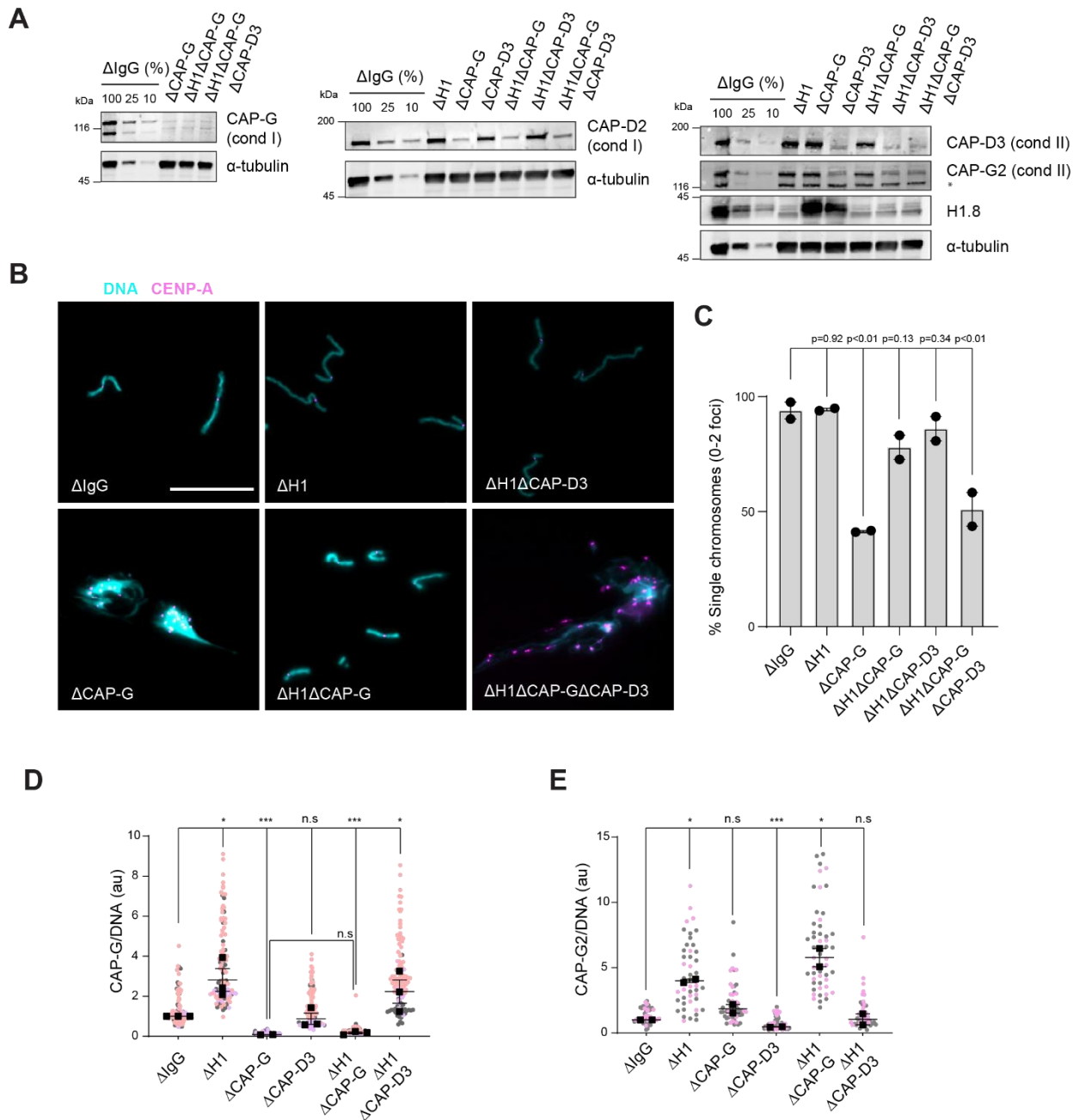
Figure 5. H1.8 suppresses condensin to limit chromosome individualization

A) Western blots showing depletion levels of condensin I and condensin II using the CAP-G and CAP-D3 antibodies respectively. B) Representative images of chromosomes after extract dilution, which disperses individualized chromosomes. DNA and centromere-associated CENP-A immunofluorescence are shown. Bar, 20 µm. C) Percent frequency of individualized chromosomes (thread-shaped DNA masses with 0-2 CENP-A foci) in the indicated conditions. A large majority of DNA masses with no CENP-A foci are derived from ΔCAP-D3 extracts, where CENP-A loading is compromised (Bernad et al., 2011). D) Quantification of CAP-G (condensin I) immunofluorescence normalized to the DNA signal for the indicated conditions. Each grey or orange dot represents the average signal intensity of a single chromosome cluster (from one nucleus). Each black dot represents the median signal intensity from a single experiment. Bars represent mean and range of the medians of two independent experiments. >20 nuclei were quantified for each condition in every experiment. E) Quantification of CAP-G2 (condensin II) immunofluorescence intensity, normalized to the DNA signal for the indicated conditions. Each grey or magenta dot represents the average signal intensity of a single chromosome cluster (from one nucleus). Each black dot represents the median signal intensity from a single experiment. Bars represent mean and range of the medians of two independent experiments. >20 nuclei were quantified for each condition in every experiment.

with replicated chromosomes, the dilution procedure (**Figure 3A**) resulted mostly in physically separated single chromosomes but also a small number of clumped chromosomes (**Figure 5A, S5D**). To better quantify chromosome individualization, we

measured the number of CENP-A foci per distinct chromatin mass (**Figure 5B, 5C, S5D**). Note that each centromere pair in a chromosome is counted as one focus, and we defined individualized chromosomes as DNA masses containing less than 3

CENP-A foci. Condensin I depletion (ΔCAP-G) resulted in defective chromosome individualization, suggesting that condensin I activity drives resolution of interchromosomal entanglements, and that condensin II is not sufficient to resolve these inter-chromosomal links in this background. Strikingly, co-depletion of H1.8 and condensin I (ΔH1ΔCAP-G) almost completely rescued chromosome individualization without detectable CAP-G on chromatin (**Figure 5A-D**). This apparent bypass of condensin I requirement in chromosome individualization is due to increased chromatin enrichment of condensin II in ΔH1ΔCAP-G extracts as chromosome individualization failed in the triple-depleted extracts (ΔH1ΔCAP-GΔCAP-D3) (**Figure 5E**). However, depletion of condensin II (ΔCAP-D3) alone or co-depletion of H1.8 and condensin II (ΔH1ΔCAP-D3) did not inhibit chromosome individualization (**Figure 5C, S5D**), suggesting the dispensability of condensin II in these conditions. These results show that both condensin I and condensin II can drive resolution of chromosomes in the absence of H1.8. However, in the presence of H1.8, abundant condensin I can still promote individualization by overcoming H1.8-mediated suppression, while less abundant condensin II does not seem to play a significant role in this process.
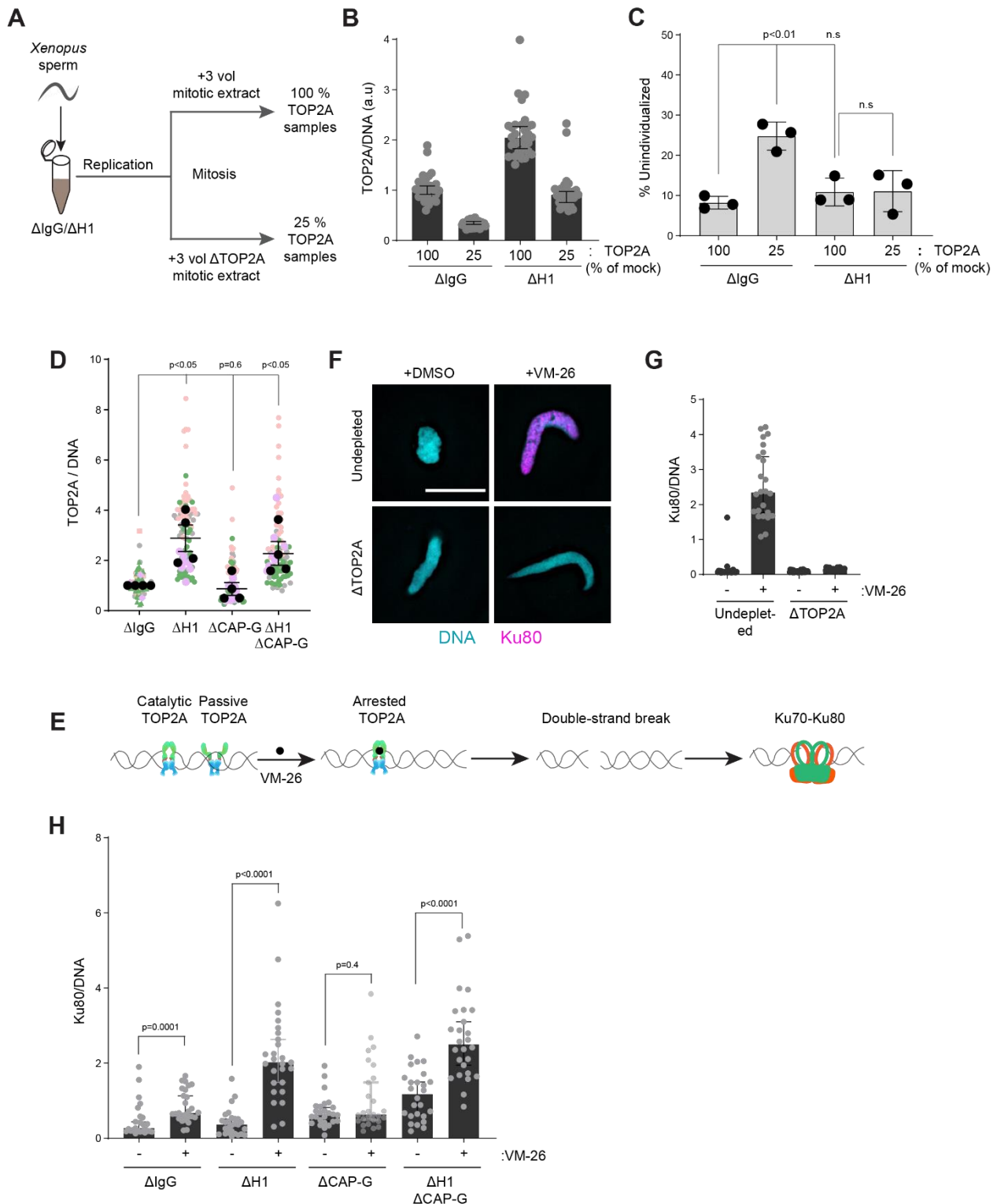
Topo II activity on mitotic chromatin is stimulated by condensin I and suppressed by H1.8

While chromosome compaction mediated by condensins facilitates decatenation and drives sister chromatid resolution (Goloborodko et al., 2016a; Nagasaka et al., 2016; Piskadlo et al., 2017), condensins also enable resolution of interchromosomal entanglements (**Figure 5**)(Sun et al., 2018). Loop extrusion by condensin also drives resolution of topo II mediated entanglements in yeast minichromosomes (Dyson et al., 2020). Since topological entanglements persist in *Xenopus* extract chromosomes (**Figure S5A**), we asked whether condensins drive the resolution of these chromosomes through TOP2A activity. Since chromosome-associated levels of condensins and TOP2A are increased upon H1.8 depletion (**Figure 1**), we examined if the increased condensin level on chromatin reduces the minimum TOP2A levels required for chromosome individualization. Complete loss of TOP2A inhibits decompaction of sperm nuclei, a process associated with replacement of protamine with histones (Adachi et al., 1991), so we addressed this question using extracts partially

depleted of TOP2A (**Figure 6A**). We first generated nuclei with replicated chromosomes in mock-depleted extracts (ΔIgG), and then the extracts were diluted with ΔTOP2A extracts to reduce the total TOP2A level to 25 %. Under this condition, the level of chromosome-associated TOP2A also reduced to 25 % (**Figure S6A, 6B**). The chromosome clusters resulting from the dilution assay were sorted into three categories (**Figure S6B**). Using this categorization, we observe that the frequency of unindividualized chromosome clusters in ΔH1 extracts increased about 3-fold from ΔIgG extracts (**Figure 6C**). When H1.8 was co-depleted, extracts with 25% levels of TOP2A were able to support maximum level of chromosome individualization as chromosome-associated levels of TOP2A became equivalent to untreated control extracts (**Figure 6B**). These data confirm that chromosome individualization is sensitive to TOP2A levels on chromatin, and that H1.8 suppresses individualization when topo II is limiting.

We next assessed if H1.8 limits TOP2A activity. While condensin is thought to promote TOP2A-dependent decatenation through introducing positive supercoils (Baxter et al., 2011), condensin I depletion (ΔCAP-G) did not affect topo II levels on chromosomes (**Figure 6D**), as previously shown (Hirano et al., 1997). In addition, TOP2A activity on unreplicated small circular DNA substrates has been previously reported to be independent of condensin (Cuvier and Hirano, 2003). We also did not see any effect of H1.8 and condensin I depletion on chromatinized kinetoplast decatenation (**Figure S6D-F**). However, it is possible that condensin I cannot form functional DNA loops in these short (~ 3 kb) circular plasmids chromatinized in *Xenopus* egg extracts. Therefore, it remains to be established if TOP2A activities are regulated by H1.8 and condensin I during mitotic chromosome compaction and individualization in *Xenopus* egg extracts. To address this question, we developed an assay to measure the TOP2A activity directly on sperm chromatin. VM-26 (teniposide) is a topo II poison that arrests catalytically active topo II in a covalent complex with DNA known as Top2cc (Long, 1992; Pommier et al., 2010). Top2cc is processed into a double-strand break by TDP2 (Ledesma et al., 2009; Schellenberg et al., 2017). These double-strand breaks can then be measured by assessing chromatin bound Ku70-Ku80 complex (Mimori and Hardin, 1986) (**Figure 6E**). To verify if we can observe TOP2A-dependent Ku80 accumulation on DNA, we incubated sperm nuclei in untreated or ΔTOP2A CSF

Choppakatla et al., Dec 2020-preprint copy- BioRxiv

Figure 6. Topo II activity on mitotic chromosomes is stimulated by condensin I and suppressed by H1.8

A) Schematic of partial TOP2A depletion to test sensitivity of chromosome individualization to TOP2A levels. B) Quantification of chromosome-associated TOP2A upon partial TOP2A depletion. Each dot represents the mean of TOP2A intensity normalized to DNA intensity of a single chromosome cluster (from one nucleus). The data plotted is median +/- 95 % C.I. >20 nuclei were quantified for each condition. C) Percent frequency of DNA clusters categorized as unindividualized nuclei upon partial TOP2A depletion. Mean and S.E.M from three independent experiments. >100 chromosomes/clusters were quantified for each condition in every experiment. D) Quantification of TOP2A immunofluorescence intensity normalized to the DNA signal for the indicated conditions. Each grey or magenta dot represents the average signal intensity of a single chromosome cluster (from one nucleus). Each grey, magenta, orange or grey dot represents the median signal intensity from a single experiment. Mean and S.E.M of the median of four independent experiments are also shown. >20 nuclei were quantified for each condition in every experiment. E) Schematic of VM-26 assay to detect topo II-dependent DNA breaks on chromatin using Ku80 immunofluorescence. F) Representative images of DNA and Ku80 immunofluorescence on sperm nucleus in indicated conditions. Bar, 10 µm. G) Quantification of Ku80 immunofluorescence signals on mitotic chromatin in F). Data is median and 95% C.I. >20 nuclei were quantified for each condition. H) VM-26-dependent Ku80 accumulation on mitotic chromatin under indicated conditions. Each dot is average of Ku80 immunofluorescence signal (normalized with DNA) of a single chromosome cluster (from one nucleus). Median and 95% C.I are shown. >20 nuclei were quantified for each condition.

extracts and measured the accumulation of Ku80 on chromosomes upon treatment with VM-26 (**Figure 6F**). Sperm chromosomes from undepleted extracts accumulated Ku80 upon VM-26 treatment in a dose dependent manner and this accumulation was entirely abrogated in the ΔTOP2A extracts (**Figures 6G and S6C**). These data demonstrate that VM-26-induced Ku80 signals report TOP2A activity in *Xenopus* egg extracts. We then applied this assay to assess the effect of depleting H1.8 and/or condensin I on TOP2A activity. Consistent with the increase in chromatin associated TOP2A, H1.8 depletion (ΔH1) increased VM-26-induced Ku80 accumulation (**Figure 6H**), while condensin I depletion (ΔCAP-G) suppressed VM-26-induced Ku80 accumulation, and H1.8 co-depletion (ΔH1ΔCAP-G) rescued the Ku80 accumulation. These data suggest that TOP2A activity is enhanced by condensin I and suppressed by H1.8.

We note that while H1.8 depletion, which increased chromosome-associated TOP2A and condensins, did not cause Ku80 accumulation without VM-26, condensin I depletion slightly increased chromosome-associated Ku80 levels in the absence of VM-26 (**Figure 6H**). Since VM-26 did not induce Ku80 accumulation in condensin I depleted extracts, we speculate that condensin I may suppress DNA breaks in a manner independent of TOP2A. Intriguingly, co-depletion of H1 and condensin I further enhanced chromosome association of Ku80 without VM-26 treatment. Although reducing H1.8 levels decreased the minimum levels of condensins needed to support chromosome individualization (**Figure 5**), these data suggest that higher condensin I levels are needed to prevent formation of DNA breaks. DNA damage in mitosis also appears to inhibit loading of condensins (Boteva et al., 2020), suggesting a possible antagonistic relationship between condensins and DNA breaks in mitosis.

Discussion

Although condensins and topo II are activated in mitosis to play essential roles in chromosome segregation (Hirano and Mitchison, 1991; Kimura et al., 1998), here we demonstrated that the abundant linker histone suppresses the loading of condensins and topo II onto chromatin in mitosis to tune chromosome length and suppress individualization (**Figure 7**).

Nucleosomes reduce binding of condensins to DNA *in vitro* (Kong et al., 2020), *in vivo* (Sutani et al., 2015) and in *Xenopus* egg extracts (Shintomi et al., 2017; Zierhut et al., 2014). Now we showed that linker histones limit binding of condensin I and II to chromatin both *in vitro* and in *Xenopus* egg extracts. H1.8 suppressed condensin binding on both mononucleosomes and nucleosome arrays, suggesting that H1.8 is able to compete out condensins for the same linker DNA targets, though the capacity of linker histones to promote higher order structures or phase separation may also limit the access of condensin (Gibson et al., 2019; Song et al., 2014). We propose that titrating linker histone amounts on chromatin could serve as a rheostat to control chromosome length (**Figure 7**).

Since the loop size is an aggregate of loop extrusion rate, processivity and number of loop extruders (Goloborodko et al., 2016b), it is unclear from our data whether H1.8 affects the loop extrusion kinetics of a single condensin molecule. However, our observation is consistent with the *in silico* simulation showing that increasing the number of loop extruders makes chromosomes thinner and longer by reducing average loop size (Goloborodko et al., 2016a). Similar DNA loop shortening accompanied with increased condensin I loading was also reported on integrated fission yeast genome DNA segments in mouse and human chromosomes (Fitz-James et al., 2020). Condensin binding is similarly suppressed by nucleosomes, but loop extrusion proceeds unhindered through sparsely distributed nucleosomes (Kong et al., 2020). Similarly, H1.8 may reduce the number of condensin molecules on chromatin but may not necessarily inhibit their processivity such that long DNA loops can be supported in the presence of H1.8. In contrast, these results seem contradictory to the classic observation where chromosomes become wider and shorter as more condensin loads on to chromosomes in cells arrested in mitosis for hours by microtubule poisons, such as colcemid (Rieder and Palazzo, 1992; Sun et al., 2018). However, reduction of condensin I in these arrested cells makes chromosomes even wider and shorter (Gibcus et al., 2018; Ono et al., 2003; Shintomi and Hirano, 2011, **Figure 4**), suggesting that lateral expansion and axial shortening during the colcemid arrest cannot be explained by overloading of condensins, though it was also reported that condensin I, but not condensin II, is required for axial shortening of chromosomes during nocodazole arrest (Hirota et al., 2004). This apparent conundrum may be explained by condensin-independent hyper-compaction of chromatin (Samejima et al., 2018). An attractive

candidate for such a mechanism is free magnesium, as it has been suggested that increased effective concentration of free magnesium during mitotic arrest due to a gradual loss of the magnesium chelator ATP contributes to chromatin condensation (Maeshima et al., 2018). Our in vitro observation that unchelated magnesium inhibits binding of condensin suggests that increased free magnesium concentration may also affect condensin activities (**Figure S2C-E**). In contrast to drug-induced mitotic arrest in somatic cells, which leads to ATP-deprivation via mitophagy (Doménech et al., 2015), natural long arrest at meiotic metaphase II in oocytes may be equipped to prevent ATP deprivation through abundant mitochondria. Thus, suppression of condensin activities by H1.8 in oocytes may prevent formation of longer and thinner chromosomes despite the long metaphase arrest.
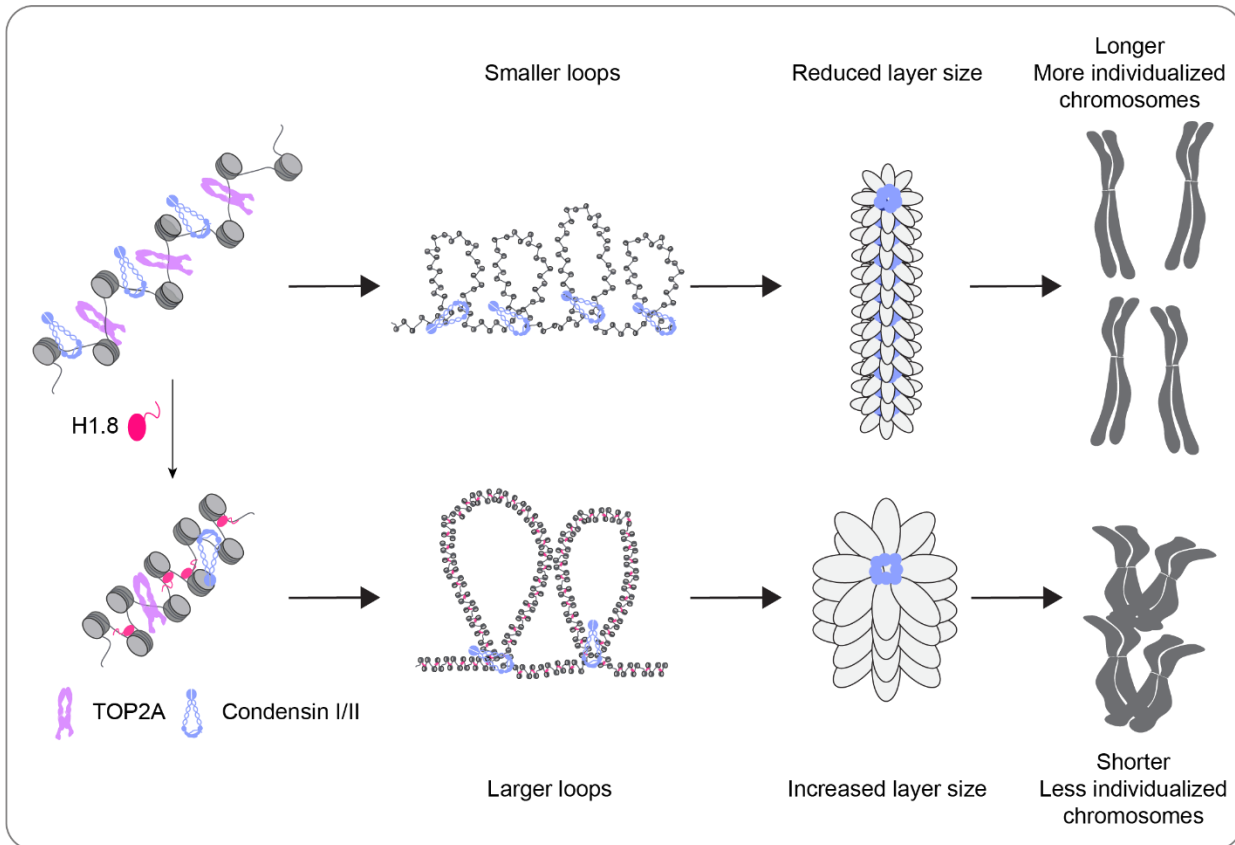
Figure 7. A graphical model of how H1.8 controls mitotic chromosome length

In the absence of H1.8, more condensins and topo II bind to more DNA loops of shorter length, resulting in longer and more individualized chromosomes (top). H1.8 limits chromatin levels of condensins and topo II to generate longer and thus fewer DNA loops, resulting in shorter and less individualized chromosomes (bottom).

The regulatory mechanisms of TOP2A recruitment to mitotic chromatin are less clear than those of condensins. TOP2A is a DNA binding protein that may also bind histone tails (Lane et al., 2013). Similar to condensin, both TOP2A and TOP2B preferentially localize at active and highly transcribed chromatin indicating a possible preference for nucleosome free regions (Canela et al., 2017; Thakurela et al., 2013; Yu et al., 2017). We observe that TOP2A levels on chromatin increase upon linker histone depletion in egg extracts and that linker histone inhibits TOP2A binding to nucleosome arrays *in vitro*, suggesting that a similar rheostat like mechanism for controlling TOP2A levels on mitotic chromatin by controlling H1 stoichiometry is possible. The preference of topo II for binding linker DNA may also explain the observation of well-spaced TOP2B binding peaks around the well-spaced nucleosomes around the CTCF- binding sites (Canela et al., 2017, 2019). However, in contrast to our finding that more TOP2A associates with elongated chromosomes in ΔH1 extracts, depletion of topo II leads to elongated chromosomes in vertebrate somatic cell lines and in early embryos of *Caenorhabditis elegans* (Farr et al., 2014; Ladouceur et al., 2017; Nielsen et al., 2020; Samejima et al., 2012). It is unclear whether these observations suggest that increased topo II activity

would lead to shorter chromosomes. One possibility is that impaired decatenation due to reduced topo II may interfere with condensin-mediated loop formation, leading to shorter loop size and thinner chromosomes as reported. On the other hand, excess topo II on chromatin, as seen in ΔH1 extracts, may not affect chromosome shape.

We also showed that condensins and topo II combine to resolve extensive and persistent interchromosomal topological entanglement during mitotic compaction in *Xenopus* egg extracts (**Figure S5**). In HeLa cells, some variants of H1 are phosphorylated and evicted along the inter-chromatid axis. This partial H1 eviction in prophase seems to be required for complete decatenation along the chromosome arms (Krishnan et al., 2017). This suggests that local enrichment of condensin II upon H1 eviction may play a role in sister chromatid decatenation. Therefore, it might be counterintuitive that activities of condensins and topo II must be limited during mitosis in egg extracts by H1.8 to suppress chromosome individualization. Since spindle assembly in oocytes relies on chromatin-induced microtubule nucleation (Heald et al., 1996), keeping chromosomes at metaphase plate might be important for maintaining robust bipolar spindle. Clustering chromosomes through incomplete individualization may also avoid generation of chromosomes that do not associate with the spindle. Such a mechanism may be particularly important during early embryonic cell divisions when the spindle checkpoint cannot be activated by unattached chromosomes (Gerhart et al., 1984; Hara et al., 1980; Mara et al., 2019). Another possible reason for the suppressed individualization is related to the fact that oocyte chromosomes completely lose cohesion from arms at the end of meiosis I, while maintaining sister chromatid cohesion only at the centromeres (Lister et al., 2010). Normally, this centromeric cohesion is critical for supporting the kinetochore tension to establish bipolar attachment. During long natural arrest at meiotic metaphase II, these centromeres undergo cohesion fatigue, where centromeres prematurely separate. However, proper segregation may still be accomplished due to apparent inter-chromatids DNA linkages (Gruhn et al., 2019). Resolution of these DNA linkages may be prevented by H1.8-mediated suppression of condensin and TOP2A.

Linker histones are a dynamic component of chromatin (Misteli et al., 2000). Linker histone occupancy varies widely (Woodcock et al., 2006), and can be controlled by both the linker histone variant and their posttranslational modifications (Christophorou et al., 2014; Hergeth and Schneider, 2015; Th'ng et al., 2005). We expect that changing the H1 stoichiometry on chromatin by changing the amount, subtype and/or affinity (e.g., through posttranslational modifications) of H1 affects the length and individualization of chromosomes through regulating the levels of condensins and topo II. In *Xenopus* embryos, exogenously added somatic linker histone variants, but not H1.8, are evicted from mitotic chromatin (Freedman and Heald, 2010). H1.8 is also more preferentially enriched on mitotic chromatin than on interphase chromatin in *Xenopus* egg extracts (Arimura et al., 2020), suggesting that loading of condensins and topo II to chromatin is actively limited by modulating mitotic H1 loading in oocytes and early embryos. Shortening chromosome length would reduce time and distance to complete chromosome segregation in rapidly dividing early embryonic cells. In addition, reducing the chromosome surface by shortening chromosomes may contribute to rapid completion of nuclear envelope formation. This is particularly important during early embryonic cell cycle in *Xenopus*, since the nuclear envelope encapsulates each individual chromosome in late anaphase to form the karyomere, in which DNA replication can be accomplished (Lemaitre et al., 1998). Although shorter chromosomes can be achieved by reducing the amount of condensin I, hypomorphic levels of condensin I result in accumulation of DNA damage by unknown mechanisms (**Figure 6E**). Thus, the appropriate balance of condensin I and the linker histone may be required to tune the appropriate chromosome length while suppressing DNA damage. Linker histones serve important interphase roles through regulation of transcription (Izzo et al., 2008), and the epigenetic landscape of the chromatin determines the linker histone variant on chromatin (Izzo et al., 2013; Parseghian et al., 2001; Th'ng et al., 2005). Since H1.8 competitively inhibits condensin binding in mitosis, it is tempting to speculate that linker histones also inhibit condensin II and cohesin binding in interphase. We suggest that local and global regulation of chromatin structure and function can be regulated by controlling differential expression of linker histone H1 variants and their modifications not just through promoting inter-nucleosomal interactions but also by controlling accessibility of SMC proteins and topo II.

Acknowledgments

Author Contributions

P.C. conducted all experiments except for Hi-C library preparation, which was done by B.D. P.C., B.D., J.D. and H.F. analyzed Hi-C data. E.E.C. prepared human condensin I and II complexes. P.C., E.E.C., A.V. and H.F. analyzed *in vitro* condensin binding data. P.C. and H.F. designed the experiments and wrote the paper. B.D., E.E.C. and J.D. edited the paper. A.V. commented on the paper. H.F. oversaw the entire project.

Experimental Model and Subject Details

Xenopus laevis frogs

Mature female pigmented *X. laevis* frogs (NASCO-LM00535MX) were maintained in a temperature-controlled room (16-18°C) using a recirculating water system at The Rockefeller Comparative BioScience Center (CBC). Frogs were temporarily moved to a satellite facility for ovulation and egg-laying according to protocols approved by the IACUC (Protocol number 20031).

Method Details

Antibodies

H3 was detected with ab1791 (Abcam; 1 µg/ml for western blots). H2B was detected with ab1790 (Abcam; 1 µg/ml for western blots). α-tubulin was detected with T9026 (Sigma; 1:10000 for western blots).

H1.8 was detected using anti-H1M (H1.8) antibody (Jenness et al. 2018; 1 µg/ml for western blots). Ku80 was detected with a C-terminal peptide antibody (Postow et al. 2008; 4 µg/ml for IF). Anti-TOP2A was a gift from Y. Azuma (Ryu et al. 2010; 1 µg/ml for western blots and IF). Anti-CAPD2 was a gift from T. Hirano (Hirano, Kobayashi, and Hirano 1997; 2 µg/ml for western blots). Anti-CAPG2 was a gift from S. Rankin (4 µg/ml for IF, 2 µg/ml for western blots). xCAP-G (Zierhut et al., 2014) and xCAP-D3 custom antibodies were used at 2 µg/ml for western blots and 1 µg/ml for IF.

xCAP-G antibody was also conjugated to Alexa488 using the Alexa488-NHS ester (Thermo-Fisher Scientific) using the manufacturer's instructions. The conjugated antibody was purified using the Sephadex G-25 in PD-10 desalting column (Cytiva). The conjugated antibody was dialyzed into PBS+50% glycerol and stored in aliquots at -80°C after freezing with liquid nitrogen. The labelled antibody was used at 4 µg/ml for IF.

IRDye 680LT Goat anti-Mouse IgG (H+L), IRDye 680LT Goat anti-Rabbit IgG (H+L), IRDye 800CW Goat anti-Mouse IgG (H+L) and IRDye 800CW Goat anti-Rabbit IgG (H+L) were used at 1:15000 (LI-COR Biosciences) dilution for western blots. Alexa 488, Alexa 555 and Alexa 647 conjugated secondary antibodies (Jackson Immunoresearch) were used for IF.

Antibody production

xCAP-D3 C-terminal peptide (CRQRISGKAPLKPSN) was synthesized at The Rockefeller University Proteomics Resource Center). The peptide was then coupled to the keyhole limpet hemocyanin according to the manufacturer's protocol (Thermo-Fisher Scientific) and used to immunize rabbits (Cocalico Biologicals). Antibody was purified from the immunized rabbit sera using affinity purification against the same peptide coupled to SulfoLink resin (Thermo-Fisher Scientific). The antibody was dialyzed into PBS+ 50% glycerol and stored with the addition of 0.05% sodium azide.

Xenopus egg extracts and Immunodepletion

Cytostatic Factor (CSF) arrested *X. laevis* egg extracts were generated as previously described (Murray, 1991). To generate replicated mitotic chromosomes, 0.3 mM CaCl$_2$ was added to CSF arrested extracts containing *X. laevis* sperm to cycle the extracts into interphase at 20°C. Ninety minutes

after adding CaCl$_2$, half the volume of fresh CSF extract and 40 nM of the non-degradable cyclin BΔ90 fragment were added to interphase extracts to induce mitotic entry (Glotzer et al., 1991; Holloway et al., 1993). After 60 min of incubation, extracts were processed for morphological and biochemical assessments. For all experiments involving immunofluorescence, 10 nM nocodazole was added along with the cyclin BΔ90.

For immunodepletions of 50-100 µl extracts, 250 µg/ml antibodies were conjugated to Protein-A coupled Dynabeads (Thermo Fisher Scientific) either at room temperature for 60 min or overnight at 4 °C. Mock (IgG) and H1.8 (H1) antibody beads were crosslinked using 4 mM BS$_3$ (Thermo Fisher Scientific) at room temperature for 45 min and quenched using 10 mM Tris-HCl (Sigma). All antibody beads were washed extensively using Sperm Dilution Buffer (SDB; 10 mM HEPES, 1mM MgCl$_2$, 100 mM KCl, 150 mM Sucrose) and separated from the buffer using a magnet before addition of extract. H1.8 depletions (ΔH1) were performed with two 45 min rounds of depletion at 4 °C using 2 volumes of antibody-coupled beads for each round. For condensin I and condensin II depletions, 1.5-2 volumes of xCAP-G or xCAP-D3 antibody-coupled beads were used in a single round for depletion for 60 min at 4 °C. For double depletion of condensin I and II, a single round of depletion using 1.5 volume each of xCAP-G and xCAP-D3 antibody-coupled beads was performed. For TopoII depletions (ΔTopoII), a single round of depletion was performed using 1.2 volume of anti-TopoIIα coupled antibody beads for 60 min at 4 °C. After the incubations, the beads were separated using a magnet. For cohesin depletions, 2 volumes of xSMC3 antibody beads were used in a single round for 60 min at 4 °C.

Teniposide assay

For **Figures 5 G, H** sperm nuclei were added along with DMSO/ 50 µM VM-26 to undepleted/ΔTOP2A CSF extract and incubated for 50 min at room temperature. The extract was then fixed and spun down onto coverslips for immunofluorescence. The coverslips were stained with xKu80 antibody to image Ku80 accumulation.

For **Figure 5H**, sperm nuclei were replicated in extracts depleted of indicated proteins. The extracts were then cycled back into mitosis by the addition of fresh CSF extract and 40 nM cyclinBΔ90 (Glotzer et al., 1991; Holloway et al., 1993) and split into two. 5

min after cycling back, DMSO and 20 µM VM-26 were added to each of the two vials in each depletion condition. Samples were fixed for immunofluorescence after 20 min.

Kinetoplast decatenation assay

CSF extracts co-depleted with anti-TOP2A antibody and anti-IgG, anti-H1.8 or anti-CAP-G antibody were cycled into interphase by the addition of 0.3 mM CaCl$_2$. 100 µg/ml cycloheximide (Sigma) was also added to prevent translation of cyclin B. After 40 min at 21 °C, 10 ng/µl kinetoplast DNA (TopoGEN) was added to the interphase extract and incubated for 150 min at 21 °C. The extract was then cycled back into mitosis with the addition of 1 volume of CSF extract (ΔIgG/ΔH1/ΔCAP-G) containing TOP2A. 30 µl samples were taken at the indicated time points and added into a tube containing 270 µl Stop Buffer I (20 mM Tris-Cl pH 8, 20 mM EDTA, 0.5% SDS, 0.05 mg/ml RNase A) which stops the decatenation reaction and the tube was incubated at 37 °C for 30 min. 300 µl Stop Buffer II (20 mM Tris-Cl pH 8, 20 mM EDTA, 0.5% SDS, 1 mg/ml Proteinase-K) was then added and the tube was incubated at 37 °C for 60 min. The tubes were then extracted once with Phenol-Chloroform-Isoamylalcohol and once with Chloroform and precipitated with ethanol overnight. The pellet after ethanol precipitation was resuspended in 1x TE with 0.05 mg/ml RNase A (Sigma) and incubated at 37 °C for 60 min to digest any remaining RNA. The samples were run on a 1% agarose gel and stained with SYBR-SAFE (Thermo-Fisher Scientific).

Plasmid supercoiling assay

CSF extracts depleted with anti-IgG, anti-H1.8 were cycled into interphase by the addition of 0.3 mM CaCl$_2$. 100 µg/ml cycloheximide (Sigma) was also added to prevent translation of cyclin B. After 40 min at 21 °C, 10 ng/µl relaxed circular pBlueScript DNA was added to the interphase extract. 30 µl samples were taken at the indicated time points and added into a tube containing 270 µl Stop Buffer I (20 mM Tris-Cl pH 8, 20 mM EDTA, 0.5% SDS, 0.05 mg/ml RNase A) which stops the decatenation reaction and the tube was incubated at 37 °C for 30 min. 300 µl Stop Buffer II (20 mM Tris-Cl pH 8, 20 mM EDTA, 0.5% SDS, 1 mg/ml Proteinase-K) was then added and the tube was incubated at 37 °C for 60 min. The tubes were then extracted once with phenol-chloroform-isoamylalcohol and once with

Chloroform and precipitated with ethanol overnight. The pellet after ethanol precipitation was resuspended in 1x TE with 0.05 mg/ml RNaseA (Sigma) and incubated at 37 ºC for 60 min to digest any remaining RNA. The samples were run on a 1% agarose gel in 1x TBE containing 0.5 µM chloroquine at 0.75 V/cm for 36 hours in 1x TBE containing 0.5 µM chloroquine. The gel was stained with SYBR-SAFE (Thermo-Fisher Scientific) and imaged.

Western blots

For total egg extract samples, 1 µl sample was added to 25 ul 1x sample buffer (50 mM Tris-HCl pH 6.8, 2 % SDS, 10% Glycerol, 2.5 % β-mercaptoethanol) and boiled for 10 min. Samples were spun at 8000 rpm for 3 min before gel electrophoresis and overnight transfer at 4 ºC. Blotting membranes were blocked with 4 % powdered skim-milk (Difco). Primary and secondary antibodies were diluted in LICOR Odyssey blocking buffer-PBS (LI-COR Biotechnology). Western blots were imaged on a LICOR Odyssey. Quantifications were done using Image-J.

Hi-C
Standard samples
10^6 *X. laevis* sperm nuclei were added to 150 µl interphase extract and allowed to replicate at 21 ^{0}C for 90 min. The extracts were cycled back into mitosis by adding 100 µl CSF extract, 40 nM of the non-degradable cyclin BΔ90 and 10 µM nocodazole (Sigma). After 60 min at metaphase, the samples were diluted into 12 ml of fixing solution (80 mM K-PIPES pH 6.8, 1 mM MgCl2, 1 mM EGTA, 30% glycerol, 0.1% Triton X-100, 1% formaldehyde) and incubated at room temperature with rocking for 10 min. The samples were then quenched with 690 µl 2.5 M glycine for 5 min at room temperature. The samples were then placed on ice for 15 min and then centrifuged at 6000 g at 4 ºC for 20 min. The pellet was then resuspended in 1 ml ice-cold DPBS. The tube was then centrifuged again at 13000 g for 20 min at 4 ºC. The buffer was aspirated, and the pellet was frozen in liquid nitrogen and then stored at -80 ºC.

Dispersed chromosome samples
The metaphase chromosome samples were prepared as above, but nocodazole was omitted. The metaphase extracts were diluted by adding 1.2 ml chromosome dilution buffer (10 mM K-HEPES pH 8, 200 mM KCl, 0.5 mM EGTA, 0.5 mM MgCl2, 250

mM Sucrose) and incubated at room temperature for 8 min. 6 ml fixation buffer (5 mM K-HEPES pH 8, 0.1 mM EDTA, 100 mM NaCl, 2 mM KCl, 1 mM MgCl2, 2 mM CaCl2, 0.5% Triton X-100, 20% glycerol, 1% formaldehyde) was added to the tube, mixed by rotation 10 min at room temperature. 420 ul 2.5 M glycine was added to quench the formaldehyde and the mixture was incubated for 5 min at room temperature. The samples were then placed on ice for 15 min and then centrifuged at 6500 g at 4 ºC for 20 min. The pellet was then resuspended in 1 ml ice-cold DPBS. The tube was then centrifuged again at 13000 g for 20 min at 4 ºC. The buffer was aspirated, and the pellet was frozen in liquid nitrogen and then stored at -80 ºC.

Library prep and sequencing
Hi-C protocol was performed as previously described (Belaghzal et al., 2017), with exception that cell disruption by douncing was omitted. Briefly, pellets were digested by DpnII overnight at 37 °C prior to biotin fill-in with biotin-14-dATP for 4 h at 23 °C. After ligation at 16 °C for 4 h, crosslinking was reversed by proteinase K at 65°C overnight. Purified ligation products were sonicated with 200 bp average size, followed by 100-350 bp size selection. End repair was performed on size selected ligation products, prior to purifying biotin tagged DNA fragments with streptavidin beads. A-tailing was done on the purified DNA fragments followed by Illumina Truseq adapter ligation. Hi-C library was finished by PCR amplification and purification to remove PCR primers. Final library was sequenced on Illumina HiSeq 4000 with PE50.

Hi-C Data Processing
Hi-C fastq files were mapped to the *Xenopus laevis* 9.2 genome with the distiller-nf pipeline (https://github.com/open2c/distiller-nf). The reads were aligned with bwa-mem, afterwards duplicate reads were filtered out. These valid pair reads were aggregated in genomic bins of 10, 25, 50, 100, 250, 500kb using the cooler format (Abdennur and Mirny, 2020). Cooler files were balanced using Iterative balancing correction (Imakaev et al., 2012), ignoring first two diagonals to avoid artifacts within the first bin such as re-ligation products. Contact heatmaps from balanced cooler files were viewed and exported with Higlass (Kerpedjiev et al., 2018).

Contact Probability (P(s)) and derivatives
Contacts probability were calculated by contact frequency (*P*) as function of genomic distance (*s*). Interaction pairs were selected for genomic distance from 1kb till 100mb binned at log-scale. Within each

genomic bin observed number of interactions were divided by total possible number of interactions within the bin. Distance decay plots were normalized by total number interactions, derivative plots were made from corresponding *P(s)*.

Immunofluorescence

Immunofluorescence was performed according to previously published protocols (Desai et al., 1998). 10 µl metaphase extracts containing chromosomes were diluted into 2 ml of fixing solution (80 mM K-PIPES pH 6.8, 1 mM MgCl$_2$, 1 mM EGTA, 30% glycerol, 0.1% Triton X-100, 2% formaldehyde) and incubated at room temperature for 7 min. The fixed chromosomes were then laid onto a cushion (80 mM K-PIPES pH 6.8, 1 mM MgCl$_2$, 1 mM EGTA, 50% glycerol) with a coverslip placed at the bottom of the tube and centrifuged at 5000g for 15 min at 18 °C in a swinging bucket rotor. The coverslips were recovered and fixed with methanol (-20 °C) for 4 min. The coverslips were then blocked overnight with antibody dilution buffer (50 mM Tris-Cl pH 7.5, 150 mM NaCl, 2% BSA). Primary and secondary antibodies were diluted in antibody dilution buffer and sealed in Prolong Gold AntiFade mounting media (Thermo-Fisher Scientific).

For coverslips stained with Alexa488-anti-CAP-G antibody (**Figure 1B, 4E, 5A, S5A, 6B**), coverslips stained with primary and secondary antibodies were washed three times with PBS-T (1x PBS +0.5% Tween-20). Then, they were blocked with 100 µg/ml rabbit IgG or 30 min and were incubated with Alexa488-anti-xCAP-G antibody without any washing steps in between. The coverslips were then washed three times with PBS-T and then sealed in Prolong Gold AntiFade mounting media (Thermo-Fisher Scientific).

Chromosome individualization

Chromosome dilution was performed as before with some modifications (Funabiki and Murray, 2000). 40 µl Chromosome Dilution Buffer (10 mM K-HEPES pH 8, 200 mM KCl, 0.5 mM EGTA, 0.5 mM MgCl$_2$, 250 mM Sucrose) was added to 10 µl metaphase extract containing chromosomes and incubated at room temperature for 8 min. 200 ul fixation buffer (5 mM K-HEPES pH 8, 0.1 mM EDTA, 100 mM NaCl, 2 mM KCl, 1 mM MgCl$_2$, 2 mM CaCl$_2$, 0.5% Triton X-100, 20% glycerol, 2% formaldehyde) was added to the tube and incubated for 10 min at room temperature. The samples were laid over a cushion (5

mM K-HEPES pH 8, 0.1 mM EDTA, 100 mM NaCl, 2 mM KCl, 1 mM MgCl$_2$, 2 mM CaCl$_2$, 50 % glycerol) with a coverslip placed under the cushion and centrifuged at 7000g for 20 min at 18 °C in a swinging bucket rotor. The coverslips were recovered and fixed with ice-cold methanol for 4 min, washed extensively and blocked overnight with antibody dilution buffer (50 mM Tris-Cl pH 7.5, 150 mM NaCl, 2% BSA).

Chromosome purification

One volume of metaphase extracts with ~3000/µl sperm nuclei was diluted into 3 volumes of DB2 (10 mM K-HEPES, 50 mM β-glycerophosphate, 50 mM NaF, 20 mM EGTA, 2 mM EDTA, 0.5 mM spermine, 1 mM phenylmethylsulfonyl fluoride, 200 mM sucrose) and laid over 1 ml cushion (DB2 with 50% sucrose). The tube was centrifuged in a swinging bucket rotor at 10,000g for 30 min at 4 °C. Most of the cushion was aspirated and the pellet was resupended in the remaining solution and transferred to a fresh tube. The sample was centrifuged again at 13000g for 15 min at 4 °C. The pellet was then resuspended in 1x sample buffer and boiled for 10 min before being subject to gel electrophoresis.

Image acquisition and analysis

All the quantitative immunofluorescence imaging and some of the spindle imaging was performed on a DeltaVision Image Restoration microscope (Applied Precision) which is a wide-field inverted microscope equipped with a pco.edge sCMOS camera (pco). The samples were imaged with z-sections of 200 nm width with a 100x (1.4 NA) objective and were processed with a iterative processive deconvolution algorithm using the SoftWoRx (Applied Precision).

The maximum intensity single slice was selected, background subtraction was performed, and average intensities were calculated on a mask generated using the DNA signal. The analysis was performed using MATLAB (Mathworks) code.

For surface area measurements, images were interpolated into stacks of 67 nm width. A surface mask was built in three-dimensional space and surface area and DNA signal was calculated using the regionprops3 MATLAB function.

Chromosome length measurements were done on a single maximum intensity slice in ImageJ 1.52p.

Mononucleosomes and nucleosome arrays

Nucleosome arrays were prepared as previously noted (Guse et al., 2011; Zierhut et al., 2014). The plasmid pAS696 which contains 19 repeats of the Widom 601 nucleosome position sequence (Lowary and Widom, 1998) was digested with EcoRI, XbaI, HaeII and DraI. The fragment containing the array was isolated using polyethylene glycol-based precipitation. The ends of the DNA fragment were filled in with dATP, dGTP, dCTP and Bio-16-dUTP (Chemcyte) using Klenow DNA polymerase (NEB) and purified using Sephadex G-50 Nick columns (Cytiva Biosciences).

Mononucleosomal DNA were prepared by digesting pAS696 using AvaI. The 196 bp fragment was isolated using polyethylene glycol-based precipitation. The ends of the fragment were filled in with dATP, dGTP, dTTP and Alexa647-aha-dCTP (Thermo-Fisher Scientific) using Klenow DNA polymerase (NEB) and purified using Sephadex G-50 Nick columns (Cytiva Biosciences).

For nucleosome deposition, 10 µg of DNA arrays or mononucleosomal DNA was mixed with equimolar amount of *X. laevis* H3-H4 tetramer and twice equimolar amount of *X. laevis* H2A-H2B dimers in 1x TE with 2 M NaCl. The mixture was added into in a Slide-A-Lyzer dialysis cassette (Thermo-Fisher Scientific) and placed into 500 ml High salt buffer (10 mM Tris-Cl pH 7.5 @ 4 °C, 2M NaCl, 1 mM EDTA, 5 mM β-mercaptoethanol, 0.01 % Triton X-100). Salt was reduced in a gradient by pumping in 2 L of Low salt buffer (10 mM Tris-Cl pH 7.5 at 4 °C, 100 mM NaCl, 1 mM EDTA, 5 mM β-mercaptoethanol, 0.01 % Triton X-100) at constant volume at 1 ml/min. The quality of the nucleosome arrays was ascertained by digesting the nucleosome arrays with AvaI overnight in low magnesium buffer (5 mM potassium acetate, 2 mM Tris-acetate, 0.5 mM magnesium acetate, 1 mM DTT, pH 7.9) and electrophoresed in a 5% polyacrylamide gel made in 0.5x TBE (45 mM Tris-borate, 1 mM EDTA). The mononucleosomes were assayed by direct electrophoresis.

Nucleosome binding assays

Nucleosome arrays were bound to M280 Streptavidin DynaBeads (Thermo-Fisher Scientific) in chromatin bead binding buffer (50 mM Tris-Cl pH 8, 150 mM NaCl, 0.25 mM EDTA, 0.05% Triton X-100, 2.5 % polyvinylalcohol) by shaking at 1300 rpm for 3.5 h. To block the Step tagged condensin complexes from binding the unconjugated streptavidin on the beads during the condensin pull downs, the beads were washed once in chromatin binding buffer and then incubated in 1 mM Biotin in chromatin binding buffer by shaking at 1300 rpm for 1 hour. The beads were then washed with chromatin binding buffer (50 mM Tris-Cl pH 8, 150 mM NaCl, 0.25 mM EDTA, 0.05% Triton X-100) three times, moved to a new tube, washed twice with SDB (10 mM HEPES, 1mM MgCl$_2$, 100 mM KCl, 150 mM Sucrose) and split into two tubes. SDB with 0.0008% poly-glutamic acid (Sigma)(Stein and Künzler, 1983) was mixed with 400 nM recombinant xH1.8 (buffer for control) and incubated for 5 min at room temperature. This mixture was incubated with the beads (half with buffer, half with xH1.8) with rotation at 16 °C. The beads were then washed 1x with SDB and 1x with binding buffer (10 mM HEPES pH 8, 40 mM NaCl, 2.5 mM MgCl$_2$, 0.5 mM DTT, 0.05% Triton X-100). Beads were washed 2x with binding buffer with indicated assay salt concentration and resuspended in binding buffer with 100 nM recombinant TOP2A, 380 nM human condensin I, condensin I Q loop mutant or 320 nM condensin II or condensin II Q loop mutant. The beads were rotated at room temperature for 30 min. Total reaction samples were taken and the beads were washed three times on a magnet in binding buffer and moved to a new tube. The beads were collected on a magnet and resuspended in 1x sample buffer (50 mM Tris-HCl pH 6.8, 2 % SDS, 10% Glycerol, 2.5 % β-mercaptoethanol) and boiled for 5 min. Gel electrophoresis was performed and the gels were stained with GelCode Blue Stain reagent (Thermo-Fisher Scientific).

Condensin Gel Shift assays

200 nM Alexa 647 labelled 196 bp mononucleosomes were mixed with 0.0008% poly-glutamic acid (Sigma)(Stein and Künzler, 1983) and half was mixed with 400 nM recombinant xH1.8 in 1x binding buffer (10 mM HEPES pH 8, 50 mM NaCl, 2.5 mM MgCl$_2$, 5 mM ATP, 0.5 mM DTT, 0.05% Triton X-100) and incubated for 30 min at room temperature. 100 nM of the mononucleosomes with or H1.8 were mixed with the indicated concentration of condensin I in 1x binding buffer at 4 °C for 30 min and subject to electrophoresis onto a 5 % polyacrylamide gel in 0.5x TBE at room temperature. The gels were imaged on a LICOR Odyssey (LI-COR Biotechnology). The binding curves were fitted using Graphpad Prism 8.4.3 using the sigmoidal binding curve option of the non-linear curve fitting.

Protein purification

H1.8

A pET51b vector expressing *Xenopus laevis* H1.8 with an N-terminal Strep-Tag II and C-terminal 6x Histidine-tag was a gift from Rebecca Heald (UC Berkeley). *E. coli* Rosetta2 (DE3 pLysS) cells containing expression plasmids were grown in TBG-M9 media (15 g/l tryptone, 7.5 g/l yeast extract, 5 g/l NaCl, 0.15 g/l MgSO$_4$, 1.5 g/l NH$_4$Cl, 3 g/l KH$_2$PO$_4$, 6 g/l Na$_2$HPO$_4$; 0.4% glucose) at 37 ^{o}C until they reach OD~0.6 and were supplemented with 1 mM isopropylthio-β-galactoside (IPTG) and grown at 18 ^{o}C for 14 h. Cells were collected and resuspend in lysis buffer (1x PBS, 500 mM NaCl, 10% glycerol, 20 mM Imidazole, 0.1% Triton X-100, 10 mM β-mercaptoethanol, 1 mM phenylmethylsulfonyl fluoride, 10 µg/ml leupeptin, 10 µg/ml pepstatin, 10 µg/ml chymostatin). All subsequent steps were carried out at 4 ^{o}C. After 30 min incubation, the cell suspension was sonicated and centrifuged at 45000g for 45 min at 4 ^{o}C. The supernatant was added to Ni-NTA beads (BioRad) and rotated for 60 min. The beads were then washed with Wash Buffer 1 (1x PBS, 20 mM imidazole, 500 mM NaCl, 4 mM β-mercaptoethanol, 10 mM ATP, 2.5 mM MgCl$_2$, cOmplete EDTA-free protease inhibitor cocktail-Roche). The beads were eluted with NTA elution buffer (1x PBS, 400 mM Imidazole, 500 mM NaCl). The correct fractions were collected and dialyzed into PBS supplement with 500 mM NaCl, concentrated using Amicon Ultra centrifugal filters (10k cutoff), flash frozen, aliquoted and stored at -80 ^{o}C.

TopoIIα

X. laevis TOP2A tagged with calmodulin binding protein (CBP) was purified from *P. pastoris* yeast as reported (Ryu et al., 2010) with some modifications. *Pichia pastoris* integrated with a CBP tagged TOP2A cassette under the influence of an alcohol oxidase (AOX) promoter (a gift from Yoshiaki Azuma) were grown in BMGY media (1% Yeast Extract, 2% Peptone, 100 mM potassium phosphate pH 6, 1.34% Yeast Nitrogen Base, 4x10^{-5}% biotin, 1% glycerol) containing 50 µg/ml G418 (Thermo-Fisher Scientific) at 30 ^{o}C until OD~4.0. The cells were collected by centrifugation and split into BMMY media (1% Yeast Extract, 2% Peptone, 100 mM potassium phosphate pH 6, 1.34% Yeast Nitrogen Base, 4x10^{-5}% biotin, 0.5% methanol) and grown at 22 ^{o}C for 14 h. The cells were collected, packed into

a syringe and extruded into liquid nitrogen in the form of noodles. These frozen noodles were lysed using a Retsch PM100 cryomill (Retsch) with continuous liquid nitrogen cooling. The cyromilled cells were then resuspended in Lysis Buffer (150mM NaCl, 18mM β-glycerophosphate, 1mM MgCl$_2$, 40mM HEPES (pH 7.8), 5% glycerol, 0.1% Triton X-100, 1mM DTT, cOmplete EDTA-free protease inhibitor tablet) and sonicated on ice. The cells were centrifuged at 35,000g for 45 min at 4 ^{o}C. 2 mM CaCl$_2$ was added to the supernatant along with Calmodulin-sepharose beads (Strategene) and the mixture was incubated at 4 ^{o}C for 120 min. The beads were then washed with ATP-Wash Buffer (Lysis Buffer+ 5mM MgCl$_2$, 2mM CaCl$_2$, 1mM ATP), Wash Buffer 1 (Lysis Buffer + 2 mM CaCl$_2$), Wash Buffer 2 (300mM NaCl, 1mM MgCl$_2$, 2mM CaCl$_2$, 20mM HEPES (pH 7.8), 5% Glycerol, 1mM DTT) and then eluted into Elution Buffer (300mM NaCl, 1mM MgCl$_2$, 5mM EGTA, 20mM HEPES (pH 7.8), 5% glycerol, 1mM DTT).

The eluted protein was then passed through a MonoQ anion exchange column (Cytiva) on an AKTA-FPLC (Cytiva) to separate co-purified DNA. The flowthrough was then digested with TEV protease to cleave the CBP tag and then loaded on a HiTrap Heparin HP column (Cytiva) on an AKTA-FPLC and eluted using a salt gradient of 150 mM NaCl to 1 M NaCl. The selected fractions were then loaded on a Superose 6 gel filtration column (Cytiva) and eluted in Freezing buffer (250mM NaCl, 1mM MgCl$_2$, 20mM HEPES pH 7.8, 5% glycerol, 1mM DTT). The protein was then concentrated and frozen in aliquots at -80 ^{o}C.

Condensins

Human condensin complexes were purified as described previously (Kong et al., 2020). Briefly, the five subunits of human condensin I and II, sub-complexes and Q-loop mutations and were assembled into biGBac vectors (Weissmann et al., 2016) to create baculovirus for protein expression in HighFive insect cells. Cell were lysed in condensin purification buffer (20 mM HEPES [pH 8], 300 mM KCl, 5 mM MgCl$_2$, 1 mM DTT, 10% glycerol) supplemented with Pierce protease inhibitor EDTA-free tablet (Thermo Scientific) and Benzonase (Sigma). Cleared lysate was loaded on to a StrepTrap HP (GE), washed with condensin purification buffer and eluted with condensin purification buffer supplemented with 5 mM Desthiobiotin (Sigma). Protein containing fractions were pooled, diluted 2-fold with Buffer A (20 mM HEPES [pH 8], 5 mM

MgCl$_2$, 5% glycerol, 1 mM DTT), loaded on to HiTrap Heparin HP column (GE), washed with Buffer A with 250 mM NaCl, then eluted with buffer A with 500 mM NaCl. Finally, size exclusion chromatography was performed using Condensin purification buffer and a Superose 6 16/70 or increase 10/300 column (GE).

Quantification and statistical analysis

All statistical analysis was performed using in-built functions in GraphPad Prism (v8.4.3). The significance analysis was performed using an unpaired students t-test in **Figures 1D, E, 1G, 2D, 3D, 5C, 5D, 5E, 6C, 6D**. The data in **Figures S3A, S3B, 6H** were analyzed by a two-tailed Mann-Whitney test.

For the CENP-A foci counting in **Figure 5C**, DNA masses were identified using a DNA mask and CENP-A foci were identified in each DNA mask using an Otsu's thresholding algorithm.

For the categorization of unindividualized chromosomes in **Figure 6C**, a large area of coverslip was imaged in panels and all the observed DNA masses were counted and categorized in an unblinded fashion.

References

Abdennur, N., and Mirny, L.A. (2020). Cooler : scalable storage for Hi-C data and other genomically labeled arrays. *36*, 311–316.

Abramo, K., Valton, A., Venev, S. V, Ozadam, H., Fox, A.N., and Dekker, J. (2019). A chromosome folding intermediate at the condensin-to-cohesin transition during telophase. Nat. Cell Biol. *21*, 1393–1402.

Adachi, Y., Luke, M., and Laemmli, U.K. (1991). Chromosome assembly in vitro: topoisomerase II is required for condensation. Cell *64*, 137–148.

Alipour, E., and Marko, J.F. (2012). Self-organization of domain structures by DNA-loop-extruding enzymes. Nucleic Acids Res. *40*, 11202–11212.

Arimura, Y., Shih, R.M., Froom, R., and Funabiki, H. (2020). Nucleosome structural variations in interphase and metaphase chromosomes. BioRxiv 2020.11.12.380386.

Banigan, E.J., and Mirny, L.A. (2020). Loop extrusion: theory meets single-molecule experiments. Curr. Opin. Cell Biol. *64*, 124–138.

Baxter, J., Sen, N., López Martínez, V., Monturus De Carandini, M.E., Schvartzman, J.B., Diffley, J.F.X., and Aragón, L. (2011). Positive supercoiling of mitotic DNA drives decatenation by topoisomerase II in eukaryotes. Science (80-.). *331*, 1328–1332.

Bednar, J., Garcia-Saez, I., Boopathi, R., Cutter, A.R., Papai, G., Reymer, A., Syed, S.H., Lone, I.N., Tonchev, O., Crucifix, C., et al. (2017). Structure and Dynamics of a 197 bp Nucleosome in Complex with Linker Histone H1. Mol. Cell *66*, 384-397.e8.

Belaghzal, H., Dekker, J., and Gibcus, J.H. (2017). Hi-C 2 . 0 : An optimized Hi-C procedure for high-resolution genome-wide mapping of chromosome conformation. Methods *123*, 56–65.

Bernad, R., Sánchez, P., Rivera, T., Rodríguez-corsino, M., Boyarchuk, E., Vassias, I., Ray-gallet, D., Arnaoutov, A., Dasso, M., Almouzni, G., et al. (2011). HJURP and condensin II are required for CENP-A assembly. *192*, 569–582.

Boteva, L., Nozawa, R., Naughton, C., Samejima, K., Earnshaw, W.C., and Gilbert, N. (2020). Common Fragile Sites Are Characterized by Faulty Condensin Loading after Replication Stress. Cell Rep. *32*, 108177.

Brahmachari, S., and Marko, J.F. (2019). Chromosome disentanglement driven via optimal compaction of loop-extruded brush structures. Proc. Natl. Acad. Sci. U. S. A. *116*, 24956–24965.

Brandão, H.B., Paul, P., van den Berg, A.A., Rudner, D.Z., Wang, X., and Mirny, L.A. (2019). RNA polymerases as moving barriers to condensin loop extrusion. Proc. Natl. Acad. Sci. *116*, 20489–20499.

Canela, A., Maman, Y., Jung, S., Wong, N., Callen, E., Day, A., Kieffer-Kwon, K.R., Pekowska, A., Zhang, H., Rao, S.S.P., et al. (2017). Genome Organization Drives Chromosome Fragility. Cell *170*, 507-521.e18.

Canela, A., Maman, Y., Huang, S.N., Wutz, G., Tang, W., Zagnoli-Vieira, G., Callen, E., Wong, N., Day, A., Peters, J.-M., et al. (2019). Topoisomerase II-Induced Chromosome Breakage and Translocation Is Determined by Chromosome Architecture and Transcriptional Activity. Mol. Cell 1–15.

Christophorou, M.A., Castelo-Branco, G., Halley-Stott, R.P., Oliveira, C.S., Loos, R., Radzisheuskaya, A., Mowen, K.A., Bertone, P., Silva, J.C.R., Zernicka-Goetz, M., et al. (2014). Citrullination regulates pluripotency and histone H1 binding to chromatin. Nature *507*, 104–108.

Cremer, T., and Cremer, M. (2010). Chromosome territories. Cold Spring Harb. Perspect. Biol. *2*, 1–

23.

Cutts, E.E., and Vannini, A. (2020). Condensin complexes: understanding loop extrusion one conformational change at a time. Biochem. Soc. Trans. *0*, 1–12.

Cuvier, O., and Hirano, T. (2003). A role of topoisomerase II in linking DNA replication to chromosome condensation. J. Cell Biol. *160*, 645–655.

Cuylen, S., Blaukopf, C., Politi, A.Z., Müller-Reichert, T., Neumann, B., Poser, I., Ellenberg, J., Hyman, A.A., and Gerlich, D.W. (2016). Ki-67 acts as a biological surfactant to disperse mitotic chromosomes. Nature *535*, 308–312.

Desai, A., Murray, A.W., Mitchison, T., and Walczak, C.E. (1998). Chapter 20 The Use of Xenopus Egg Extracts to Study Mitotic Spindle Assembly and Function in Vitro. Methods Cell Biol. *61*, 385–412.

Doménech, E., Maestre, C., Esteban-Martínez, L., Partida, D., Pascual, R., Fernández-Miranda, G., Seco, E., Campos-Olivas, R., Pérez, M., Megias, D., et al. (2015). AMPK and PFKFB3 mediate glycolysis and survival in response to mitophagy during mitotic arrest. Nat. Cell Biol. *17*, 1304–1316.

Dworkin-Rastl, E., Kandolf, H., and Smith, R.C. (1994). The maternal histone H1 variant, H1M (B4 protein), is the predominant H1 histone in Xenopus pregastrula embryos. Dev. Biol. *161*, 425–439.

Dyson, S., Segura, J., Martínez-García, B., Valdés, A., and Roca, J. (2020). Condensin minimizes topoisomerase II-mediated entanglements of DNA in vivo. EMBO J. 1–14.

Earnshaw, W.C., and Laemmli, U.K. (1983). Architecture of metaphase chromosomes and chromosome scaffolds. J. Cell Biol. *96*, 84–93.

Eltsov, M., MacLellan, K.M., Maeshima, K., Frangakis, A.S., and Dubochet, J. (2008). Analysis of cryo-electron microscopy images does not support the existence of 30-nm chromatin fibers in mitotic chromosomes in situ. Proc. Natl. Acad. Sci. *105*, 19732–19737.

Farcas, A., Uluocak, P., Helmhart, W., and Nasmyth, K. (2011). Cohesin's concatenation of sister DNAs maintains their intertwining. Mol. Cell *44*, 97–107.

Farr, C.J., Antoniou-Kourounioti, M., Mimmack, M.L., Volkov, A., and Porter, A.C.G. (2014). The α isoform of topoisomerase II is required for hypercompaction of mitotic chromosomes in human cells. Nucleic Acids Res. *42*, 4414–4426.

Finch, J.T., and Klug, A. (1976). Solenoidal model for superstructure in chromatin. Proc. Natl. Acad.

Sci. *73*, 1897–1901.

Fitz-James, M.H., Tong, P., Pidoux, A.L., Ozadam, H., Yang, L., White, S.A., Dekker, J., and Allshire, R.C. (2020). Large domains of heterochromatin direct the formation of short mitotic chromosome loops. Elife *9*.

Freedman, B.S., and Heald, R. (2010). Functional comparison of H1 histones in Xenopus reveals isoform-specific regulation by Cdk1 and RanGTP. Curr. Biol. *20*, 1048–1052.

Funabiki, H., and Murray, A.W. (2000). The Xenopus chromokinesin Xkid is essential for metaphase chromosome alignment and must be degraded to allow anaphase chromosome movement. Cell *102*, 411–424.

Ganji, M., Shaltiel, I.A., Bisht, S., Kim, E., Kalichava, A., Haering, C.H., and Dekker, C. (2018). Real-time imaging of DNA loop extrusion by condensin. Science (80-.). *360*, 102–105.

Gassler, J., Brandão, H.B., Imakaev, M., Flyamer, I.M., Ladstätter, S., Bickmore, W.A., Peters, J., Mirny, L.A., and Tachibana, K. (2017). A mechanism of cohesin-dependent loop extrusion organizes zygotic genome architecture. EMBO J. *36*, 3600–3618.

Gerhart, J., Wu, M., and Kirschner, M. (1984). Cell cycle dynamics of an M-phase-specific cytoplasmic factor in Xenopus laevis oocytes and eggs. J. Cell Biol. *98*, 1247–1255.

Gibcus, J.H., Samejima, K., Goloborodko, A., Samejima, I., Naumova, N., Nuebler, J., Kanemaki, M.T., Xie, L., Paulson, J.R., Earnshaw, W.C., et al. (2018). A pathway for mitotic chromosome formation. Science (80-.). *359*.

Gibson, B.A., Doolittle, L.K., Schneider, M.W.G., Jensen, L.E., Gamarra, N., Henry, L., Gerlich, D.W., Redding, S., and Rosen, M.K. (2019). Organization of Chromatin by Intrinsic and Regulated Phase Separation. Cell 1–15.

Glotzer, M., Murray, A.W., and Kirschner, M.W. (1991). Cyclin is degraded by the ubiquitin pathway. *349*.

Golfier, S., Quail, T., Kimura, H., and Brugués, J. (2020). Cohesin and condensin extrude DNA loops in a cell-cycle dependent manner. Elife *9*.

Goloborodko, A., Imakaev, M. V., Marko, J.F., and Mirny, L.A. (2016a). Compaction and segregation of sister chromatids via active loop extrusion. Elife *5*, 1–16.

Goloborodko, A., Marko, J.F., and Mirny, L.A. (2016b). Chromosome Compaction by Active Loop Extrusion. Biophys. J. *110*, 2162–2168.

Goundaroulis, D., Lieberman Aiden, E., and

Stasiak, A. (2020). Chromatin Is Frequently Unknotted at the Megabase Scale. Biophys. J. *118*, 2268–2279.

Grigoryev, S.A., Bascom, G., Buckwalter, J.M., Schubert, M.B., Woodcock, C.L., and Schlick, T. (2016). Hierarchical looping of zigzag nucleosome chains in metaphase chromosomes. Proc. Natl. Acad. Sci. *113*, 1238–1243.

Gruhn, J.R., Zielinska, A.P., Shukla, V., Blanshard, R., Capalbo, A., Cimadomo, D., Nikiforov, D., Chan, A.C.-H., Newnham, L.J., Vogel, I., et al. (2019). Chromosome errors in human eggs shape natural fertility over reproductive life span. Science (80-.). *365*, 1466–1469.

Guacci, V., Hogan, E., and Koshland, D. (1994). Chromosome condesation and sister chromatid pairing in budding yeast. J. Cell Biol. *125*, 517–530.

Guse, A., Carroll, C.W., Moree, B., Fuller, C.J., and Straight, A.F. (2011). In vitro centromere and kinetochore assembly on defined chromatin templates. Nature *477*, 354–358.

Hara, K., Tydeman, P., and Kirschner, M. (1980). A cytoplasmic clock with the same period as the division cycle in Xenopus eggs. Proc. Natl. Acad. Sci. U. S. A. *77*, 462–466.

Hassler, M., Shaltiel, I.A., Kschonsak, M., Simon, B., Merkel, F., Thärichen, L., Bailey, H.J., Macošek, J., Bravo, S., Metz, J., et al. (2019). Structural Basis of an Asymmetric Condensin ATPase Cycle. Mol. Cell *74*, 1175-1188.e9.

Heald, R., and Gibeaux, R. (2018). ScienceDirect Subcellular scaling : does size matter for cell division ? Curr. Opin. Cell Biol. *52*, 88–95.

Hergeth, S.P., and Schneider, R. (2015). The H1 linker histones: multifunctional proteins beyond the nucleosomal core particle. EMBO Rep. *16*, 1439–1453.

Hirano, T., and Mitchison, T.J. (1991). Cell cycle control of higher-order chromatin assembly around naked DNA in vitro. J. Cell Biol. *115*, 1479–1489.

Hirano, T., and Mitchison, T.J. (1994). A heterodimeric coiled-coil protein required for mitotic chromosome condensation in vitro. Cell *79*, 449–458.

Hirano, T., Kobayashi, R., and Hirano, M. (1997). Condensins, Chromosome Condensation Protein Complexes Containing XCAP-C, XCAP-E and a Xenopus Homolog of the Drosophila Barren Protein. Cell *89*, 511–521.

Holloway, S.L., Glotzer, M., King, R.W., and Murray, A.W. (1993). Anaphase is initiated by proteolysis rather than by the inactivation of maturation-promoting factor. Cell *73*, 1393–1402.

Hopfner, K.P., Karcher, A., Shin, D.S., Craig, L., Arthur, L.M., Carney, J.P., and Tainer, J.A. (2000). Structural biology of Rad50 ATPase: ATP-driven conformational control in DNA double-strand break repair and the ABC-ATPase superfamily. Cell *101*, 789–800.

Hsieh, T.-H.S., Cattoglio, C., Slobodyanyuk, E., Hansen, A.S., Rando, O.J., Tjian, R., and Darzacq, X. (2020). Resolving the 3D Landscape of Transcription-Linked Mammalian Chromatin Folding. Mol. Cell *78*.

Imakaev, M., Fudenberg, G., McCord, R.P., Naumova, N., Goloborodko, A., Lajoie, B.R., Dekker, J., and Mirny, L.A. (2012). Iterative correction of Hi-C data reveals hallmarks of chromosome organization. Nat. Methods *9*, 999–1003.

Izzo, A., Kamieniarz, K., and Schneider, R. (2008). The histone H1 family: Specific members, specific functions? Biol. Chem. *389*, 333–343.

Izzo, A., Kamieniarz-Gdula, K., Ramírez, F., Noureen, N., Kind, J., Manke, T., vanSteensel, B., and Schneider, R. (2013). The Genomic Landscape of the Somatic Linker Histone Subtypes H1.1 to H1.5 in Human Cells. Cell Rep. *3*, 2142–2154.

Jenness, C., Giunta, S., Müller, M.M., Kimura, H., Muir, T.W., and Funabiki, H. (2018). HELLS and CDCA7 comprise a bipartite nucleosome remodeling complex defective in ICF syndrome. Proc. Natl. Acad. Sci. 201717509.

Kerpedjiev, P., Abdennur, N., Lekschas, F., Mccallum, C., Dinkla, K., Strobelt, H., Luber, J.M., Ouellette, S.B., Azhir, A., Kumar, N., et al. (2018). HiGlass : web-based visual exploration and analysis of genome interaction maps. 1–12.

Kimura, K., Hirano, M., Kobayashi, R., and Hirano, T. (1998). Phosphorylation and activation of 13S condensin by Cdc2 in vitro. Science (80-.). *282*, 487–490.

Kong, M., Cutts, E.E., Pan, D., Beuron, F., Kaliyappan, T., Xue, C., Morris, E.P., Musacchio, A., Vannini, A., and Greene, E.C. (2020). Human Condensin I and II Drive Extensive ATP-Dependent Compaction of Nucleosome-Bound DNA. Mol. Cell 683540.

Krietenstein, N., Abraham, S., Venev, S. V., Abdennur, N., Gibcus, J.H., Hsieh, T.-H.S., Parsi, K.M., Yang, L., Maehr, R., Mirny, L.A., et al. (2020). Ultrastructural Details of Mammalian Chromosome Architecture. Mol. Cell *78*.

Ladouceur, A.-M., Dorn, J.F., and Maddox, P.S. (2015). Mitotic chromosome length scales in response to both cell and nuclear size. J. Cell Biol.

209, 645–652.

Ladouceur, A.-M.M., Ranjan, R., Smith, L., Fadero, T., Heppert, J., Goldstein, B., Maddox, A.S., and Maddox, P.S. (2017). CENP-A and topoisomerase-II antagonistically affect chromosome length. J. Cell Biol. *216*, jcb.201608084.

Lane, A.B., Giménez-Abián, J.F., and Clarke, D.J. (2013). A novel chromatin tether domain controls topoisomerase IIα dynamics and mitotic chromosome formation. J. Cell Biol. *203*, 471–486.

Ledesma, F.C., El Khamisy, S.F., Zuma, M.C., Osborn, K., and Caldecott, K.W. (2009). A human 5′-tyrosyl DNA phosphodiesterase that repairs topoisomerase-mediated DNA damage. Nature *461*, 674–678.

Lemaitre, J.M., Géraud, G., and Méchali, M. (1998). Dynamics of the genome during early Xenopus laevis development: karyomeres as independent units of replication. J. Cell Biol. *142*, 1159–1166.

Li, W., Chen, P., Yu, J., Dong, L., Liang, D., Feng, J., Yan, J., Wang, P.Y., Li, Q., Zhang, Z., et al. (2016). FACT Remodels the Tetranucleosomal Unit of Chromatin Fibers for Gene Transcription. Mol. Cell *64*, 120–133.

Lieberman-Aiden, E., van Berkum, N.L., Williams, L., Imakaev, M., Ragoczy, T., Telling, A., Amit, I., Lajoie, B.R., Sabo, P.J., Dorschner, M.O., et al. (2009). Comprehensive Mapping of Long-Range Interactions Reveals Folding Principles of the Human Genome. Science (80-.). *326*, 289–293.

Lister, L.M., Kouznetsova, A., Hyslop, L.A., Kalleas, D., Pace, S.L., Barel, J.C., Nathan, A., Floros, V., Adelfalk, C., Watanabe, Y., et al. (2010). Age-related meiotic segregation errors in mammalian oocytes are preceded by depletion of cohesin and Sgo2. Curr. Biol. *20*, 1511–1521.

Lowary, P.., and Widom, J. (1998). New DNA sequence rules for high affinity binding to histone octamer and sequence-directed nucleosome positioning. J. Mol. Biol. *276*, 19–42.

Löwe, J., Cordell, S.C., and Van Den Ent, F. (2001). Crystal structure of the SMC head domain: An ABC ATPase with 900 residues antiparallel coiled-coil inserted. J. Mol. Biol. *306*, 25–35.

Maeshima, K., Matsuda, T., Shindo, Y., Imamura, H., Tamura, S., Imai, R., Kawakami, S., Nagashima, R., Soga, T., Noji, H., et al. (2018). A Transient Rise in Free Mg2+Ions Released from ATP-Mg Hydrolysis Contributes to Mitotic Chromosome Condensation. Curr. Biol. *28*, 444-451.e6.

Mara, L., Paim, G., and Fitzharris, G. (2019). Cell-Size-Independent Spindle Checkpoint Failure Underlies Chromosome Segregation Error in Mouse Report Cell-Size-Independent Spindle Checkpoint Failure Underlies Chromosome Segregation Error. 865–873.

Maresca, T.J., Freedman, B.S., and Heald, R. (2005). Histone H1 is essential for mitotic chromosome architecture and segregation in Xenopus laevis egg extracts. J. Cell Biol. *169*, 859–869.

Marko, J.F. (2008). Micromechanical studies of mitotic chromosomes. Chromosom. Res. *16*, 469–497.

Micheli, G., Luzzatto, A.R., Carrì, M.T., de Capoa, A., and Pelliccia, F. (1993). Chromosome length and DNA loop size during early embryonic development of Xenopus laevis. Chromosoma *102*, 478–483.

Mimori, T., and Hardin, J.A. (1986). Mechanism of interaction between Ku protein and DNA. J. Biol. Chem. *261*, 10375–10379.

Misteli, T., Gunjan, a, Hock, R., Bustin, M., and Brown, D.T. (2000). Dynamic binding of histone H1 to chromatin in living cells. Nature *408*, 877–881.

Murray, A.W. (1991). Chapter 30 Cell Cycle Extracts. In Methods in Cell Biology, pp. 581–605.

Nagasaka, K., Hossain, M.J., Roberti, M.J., Ellenberg, J., and Hirota, T. (2016). Sister chromatid resolution is an intrinsic part of chromosome organization in prophase. Nat. Cell Biol. *18*, 692–699.

Nasmyth, K. (2001). Disseminating the Genome: Joining, Resolving, and Separating Sister Chromatids During Mitosis and Meiosis. Annu. Rev. Genet. *35*, 673–745.

Naumova, N., Imakaev, M., Fudenberg, G., Zhan, Y.Y., Lajoie, B.R., Mirny, L.A., and Dekker, J. (2013). Organization of the Mitotic Chromosome. Science (80-.). *342*, 948–953.

Nielsen, C.F., Zhang, T., Barisic, M., Kalitsis, P., and Hudson, D.F. (2020). Topoisomerase IIa is essential for maintenance of mitotic chromosome structure. Proc. Natl. Acad. Sci. U. S. A. *117*.

Ohsumi, K., Katagiri, C., and Kishimoto, T. (1993). Chromosome condensation in Xenopus mitotic extracts without histone H1. Science (80-.). *262*, 2033–2035.

Ono, T., Losada, A., Hirano, M., Myers, M.P., Neuwald, A.F., and Hirano, T. (2003). Differential contributions of condensin I and condensin II to mitotic chromosome architecture in vertebrate cells. Cell *115*, 109–121.

Parseghian, M.H., Newcomb, R.L., and Hamkalo,

B.A. (2001). Distribution of somatic H1 subtypes is non-random on active vs. inactive chromatin II: Distribution in human adult fibroblasts. J. Cell. Biochem. *83*, 643–659.

Patel, L., Kang, R., Rosenberg, S.C., Qiu, Y., Raviram, R., Chee, S., Hu, R., Ren, B., Cole, F., and Corbett, K.D. (2019). Dynamic reorganization of the genome shapes the recombination landscape in meiotic prophase. Nat. Struct. Mol. Biol. *26*.

Paulson, J.R., and Laemmli, U.K. (1977). The structure of histone-depleted metaphase chromosomes. Cell *12*, 817–828.

Piskadlo, E., Tavares, A., and Oliveira, R.A. (2017). Metaphase chromosome structure is dynamically maintained by condensin I-directed DNA (de)catenation. Elife *6*, 1–22.

Pommier, Y., Leo, E., Zhang, H., and Marchand, C. (2010). DNA topoisomerases and their poisoning by anticancer and antibacterial drugs. Chem. Biol. *17*, 421–433.

Postow, L., Ghenoiu, C., Woo, E.M., Krutchinsky, A.N., Chait, B.T., and Funabiki, H. (2008). Ku80 removal from DNA through double strand break-induced ubiquitylation. J. Cell Biol. *182*, 467–479.

Potapova, T.A., Unruh, J.R., Yu, Z., Rancati, G., Li, H., Stampfer, M.R., and Gerton, J.L. (2019). Superresolution microscopy reveals linkages between ribosomal DNA on heterologous chromosomes. J. Cell Biol. *218*, 2492–2513.

Rieder, C.L., and Palazzo, R.E. (1992). Colcemid and the mitotic cycle. J. Cell Sci. *102 (Pt 3*, 387–392.

Riggs, A.D. (1990). DNA methylation and late replication probably aid cell memory, and type I DNA reeling could aid chromosome folding and enhancer function. Philos. Trans. R. Soc. Lond. B. Biol. Sci. *326*, 285–297.

Rosin, L.F., Nguyen, S.C., and Joyce, E.F. (2018). Condensin II drives large-scale folding and spatial partitioning of interphase chromosomes in Drosophila nuclei. PLoS Genet. *14*, 1–26.

Ryu, H., Furuta, M., Kirkpatrick, D., Gygi, S.P., and Azuma, Y. (2010). PIASy-dependent SUMOylation regulates DNA topoisomerase IIα activity. J. Cell Biol. *191*, 783–784.

Samejima, K., Samejima, I., Vagnarelli, P., Ogawa, H., Vargiu, G., Kelly, D.A., Alves, F. de L., Kerr, A., Green, L.C., Hudson, D.F., et al. (2012). Mitotic chromosomes are compacted laterally by KIF4 and condensin and axially by topoisomerase IIα. J. Cell Biol. *199*, 755–770.

Samejima, K., Booth, D.G., Ogawa, H., Paulson, J.R., Xie, L., Watson, C.A., Platani, M., Kanemaki, M.T., and Earnshaw, W.C. (2018). Functional analysis after rapid degradation of condensins and 3D-EM reveals chromatin volume is uncoupled from chromosome architecture in mitosis. *i.*

Schellenberg, M.J., Lieberman, J.A., Herrero-Ruiz, A., Butler, L.R., Williams, J.G., Muñoz-Cabello, A.M., Mueller, G.A., London, R.E., Cortés-Ledesma, F., and Williams, R.S. (2017). ZATT (ZNF451)–mediated resolution of topoisomerase 2 DNA-protein cross-links.

Shakya, A., Park, S., Rana, N., and King, J.T. (2020). Liquid-Liquid Phase Separation of Histone Proteins in Cells: Role in Chromatin Organization. Biophys. J. *118*, 753–764.

Shechter, D., Nicklay, J.J., Chitta, R.K., Shabanowitz, J., Hunt, D.F., and David Allis, C. (2009). Analysis of histones in Xenopus laevis I. a distinct index of enriched variants and modifications exists in each cell type and is remodeled during developmental transitions. J. Biol. Chem. *284*, 1064–1074.

Shintomi, K., and Hirano, T. (2011). The relative ratio of condensin I to II determines chromosome shapes service The relative ratio of condensin I to II determines chromosome shapes. Genes Dev. *25*, 1464–1469.

Shintomi, K., Inoue, F., Watanabe, H., Ohsumi, K., Ohsugi, M., and Hirano, T. (2017). Mitotic chromosome assembly despite nucleosome depletion in Xenopus egg extracts. Science *356*, 1284–1287.

Song, F., Chen, P., Sun, D., Wang, M., Dong, L., Liang, D., Xu, R.-M., Zhu, P., and Li, G. (2014). Cryo-EM Study of the Chromatin Fiber Reveals a Double Helix Twisted by Tetranucleosomal Units. Science (80-.). *344*, 376–380.

Sun, M., Biggs, R., Hornick, J., and Marko, J.F. (2018). Condensin controls mitotic chromosome stiffness and stability without forming a structurally contiguous scaffold. Chromosom. Res. *26*, 277–295.

Sundin, O., and Varshavsky, A. (1981). Arrest of Segregation Leads to Accumulation of Highly Intertwined Catenated Dimers : Dissection of the Final Stages of SV40 DNA Replication. Cell *25*, 659–669.

Sutani, T., Sakata, T., Nakato, R., Masuda, K., Ishibashi, M., Yamashita, D., Suzuki, Y., Hirano, T., Bando, M., and Shirahige, K. (2015). Condensin targets and reduces unwound DNA structures associated with transcription in mitotic chromosome condensation. Nat. Commun. *6*, 1–13.

Szabo, Q., Bantignies, F., and Cavalli, G. (2019). Principles of genome folding into topologically

associating domains. Sci. Adv. *5*.

Tavares-Cadete, F., Norouzi, D., Dekker, B., Liu, Y., and Dekker, J. (2020). Multi-contact 3C reveals that the human genome during interphase is largely not entangled. Nat. Struct. Mol. Biol. 1–44.

Terakawa, T., Bisht, S., Eeftens, J.M., Dekker, C., Haering, C.H., and Greene, E.C. (2017). The condensin complex is a mechanochemical motor that translocates along DNA. Science (80-.). *6516*, 1–10.

Th'ng, J.P.H., Sung, R., Ye, M., and Hendzel, M.J. (2005). H1 Family Histones in the Nucleus. J. Biol. Chem. *280*, 27809–27814.

Thakurela, S., Garding, A., Jung, J., Schübeler, D., Burger, L., and Tiwari, V.K. (2013). Gene regulation and priming by topoisomerase IIα in embryonic stem cells. Nat. Commun. *4*.

Umesono, K., Hiraoka, Y., Toda, T., and Yanagida, M. (1983). Visualization of chromosomes in mitotically arrested cells of the fission yeast Schizosaccharomyces pombe. Curr. Genet. *7*, 123–128.

Walther, N., Hossain, M.J., Politi, A.Z., Koch, B., Kueblbeck, M., Ødegård-Fougner, Ø., Lampe, M., and Ellenberg, J. (2018). A quantitative map of human Condensins provides new insights into mitotic chromosome architecture. J. Cell Biol. *217*, 2309–2328.

Weissmann, F., Petzold, G., VanderLinden, R., Huis in 't Veld, P.J., Brown, N.G., Lampert, F.,

Westermann, S., Stark, H., Schulman, B.A., and Peters, J.-M. (2016). biGBac enables rapid gene assembly for the expression of large multisubunit protein complexes. Proc. Natl. Acad. Sci. *113*, E2564–E2569.

White, A.E., Hieb, A.R., and Luger, K. (2016). A quantitative investigation of linker histone interactions with nucleosomes and chromatin. Sci. Rep. *6*, 1–14.

Woodcock, C.L., Skoultchi, A.I., and Fan, Y. (2006). Role of linker histone in chromatin structure and function: H1 stoichiometry and nucleosome repeat length. Chromosom. Res. *14*, 17–25.

Wühr, M., Freeman, R.M., Presler, M., Horb, M.E., Peshkin, L., Gygi, S.P., and Kirschner, M.W. (2014). Deep proteomics of the xenopus laevis egg using an mRNA-derived reference database. Curr. Biol. *24*, 1467–1475.

Yu, X., Davenport, J.W., Urtishak, K.A., Carillo, M.L., Gosai, S.J., Kolaris, C.P., Byl, J.A.W., Rappaport, E.F., Osheroff, N., Gregory, B.D., et al. (2017). Genome-wide TOP2A DNA cleavage is biased toward translocated and highly transcribed loci. Genome Res. *27*, 1238–1249.

Zierhut, C., Jenness, C., Kimura, H., and Funabiki, H. (2014). Nucleosomal regulation of chromatin composition and nuclear assembly revealed by histone depletion. Nat. Struct. Mol. Biol. *21*, 617–625.
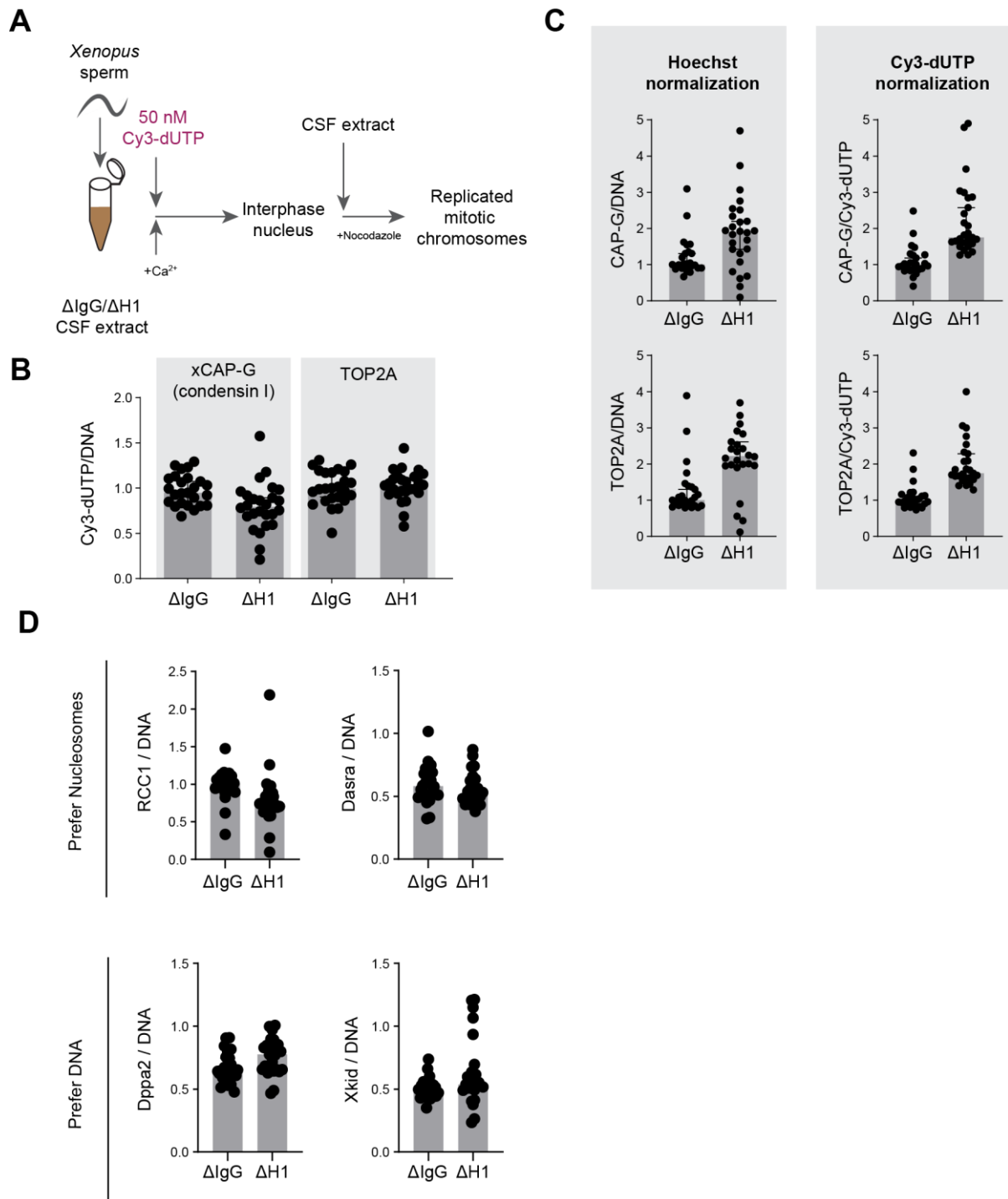
Figure S1. Linker histone H1.8 depletion does not lead to global accumulation of DNA-binding proteins (related to Figure 1)

A) Experimental scheme to incorporate Cy3-labelled nucleotides to use normalization of immunofluorescence signals on chromosomes. B) Quantification of Cy3-dUTP signals normalized to Hoechst 33342 signals, showing uniform normalization across two coverslips used for quantification of condensin I and TOP2A. The result also indicates no detectable defect in DNA replication in ΔH1 extracts. C) CAP-G (condensin I) and TOP2A immunofluorescence signal levels on chromosomes normalized with Hoechst and incorporated Cy3-dUTP. D) Quantification of immunofluorescence signal levels of two proteins that prefer nucleosomes (RCC1 and Dasra A) and two that prefer to bind nucleosome-free DNA (Dppa2 and Xkid) (Zierhut et al., 2014). In B-D, distribution of signal intensity per chromosome cluster (dots), and median and SEM from one experiment are shown. >20 nuclei were quantified for each condition plotted.

Choppakatla et al., Dec 2020-preprint copy- BioRxiv
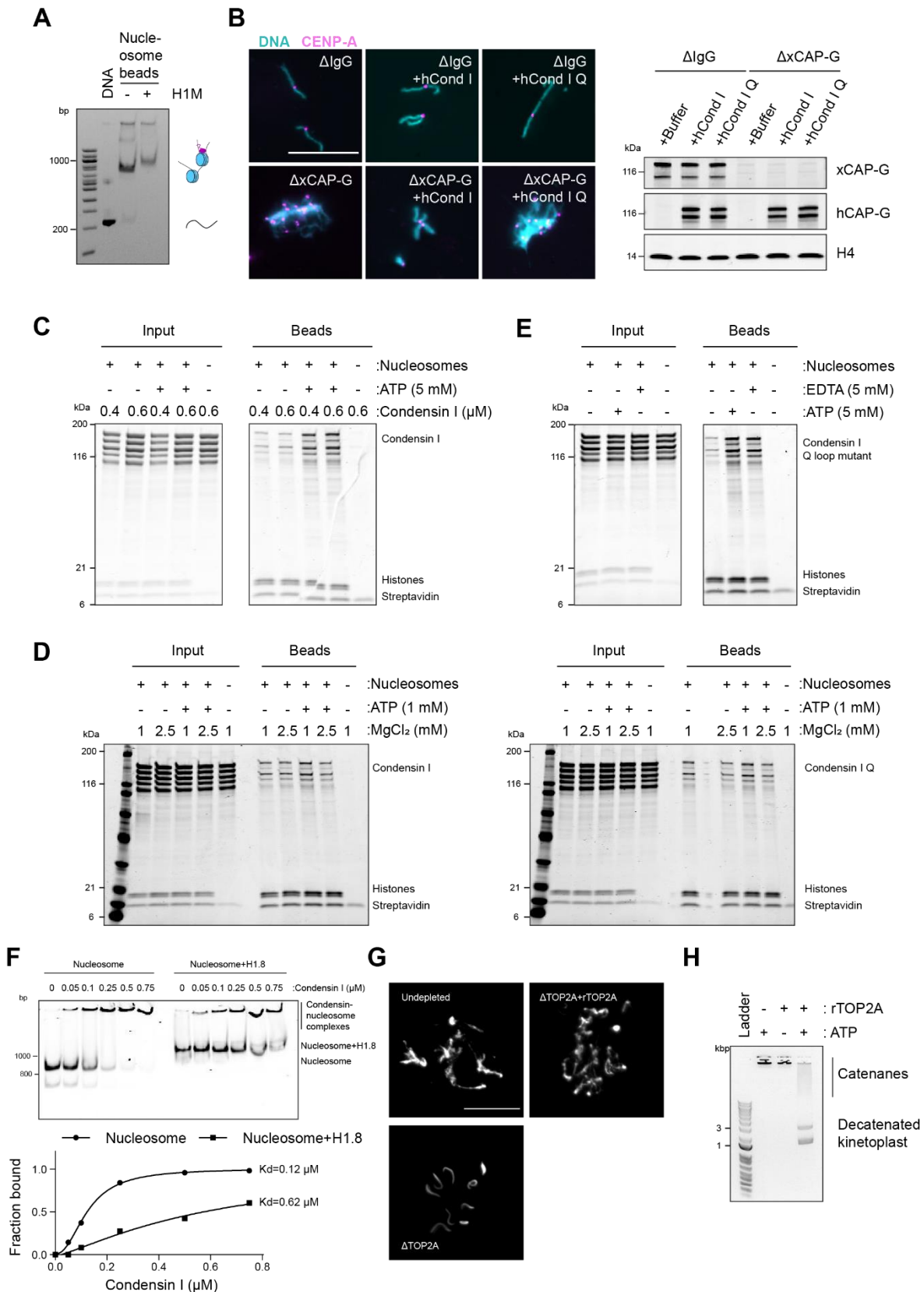
Figure S2. Linker histone inhibits binding of condensins and TOP2A (related to Figure 2)
A) Native PAGE gel analysis of nucleosome array beads loaded with or without H1.8 after digestion of the array with AvaI, which released monomers of nucleosome positioning sequence. A complete shift of monomer bands by H1.8 addition indicates the saturated occupancy of nucleosome and H1.8. B) Representative Hoechst (DNA) and CENP-A immunofluorescence images of chromosomes in indicated metaphase egg extracts after dilution, which disperses individualized chromosomes (left). Extracts depleted of condensin I (ΔCAP-G) were complemented with recombinant human condensin I and condensin I Q loop mutant protein complexes. Western blots of depletion and the rescue conditions (right). C) Purified recombinant human condensin I was incubated with nucleosome array beads in buffer containing 2.5 mM MgCl$_2$ with and without 5 mM ATP. Coomassie staining of input and bead fractions are shown.D) Purified human condensin I or condensin I Q loop mutant was incubated with nucleosome array beads in buffer containing 1 or 2.5 mM MgCl$_2$ with and without 1 mM ATP. Coomassie staining of input and bead fractions are shown.E) Purified human condensin I Q loop mutant was incubated with nucleosome array beads in buffer containing 2.5 mM MgCl$_2$ with the

addition of 5 mM ATP or 5 mM EDTA. Coomassie staining of input and bead fractions are shown. F) Alexa647-labelled 196 bp mononucleosomes with or without H1.8 were incubated with indicated concentrations of condensin I and electrophoresed on a 5 % native PAGE. Alexa647-labeled DNAs are shown. Bands at the well represent the nucleosome-condensin complex. Condensin I binding curves with mononucleosomes with and without H1.8, showing the large increase in binding constant in the presence of H1.8. Absence of signals at the well in the absence of Condensin I indicates that mononucleosomes do not form large aggregates in the presence or absence of rH1.8 under the experimental condition. G) Recombinant X. laevis TOP2A is functional in Xenopus egg extracts. Sperm nuclei were added to undepleted, TOP2A-depleted CSF extracts (ΔTOP2A), or ΔTOP2A extracts with purified recombinant TOP2A. Representative Hoechst (DNA) images of sperm are shown. In undepleted or ΔTOP2A extracts with supplemented TOP2A, proper sperm remodeling led to mitotic chromosomes formation. In ΔTOP2A extracts, sperm remodeling failed and sperm nuclei remained compact crescent-like shape. Bar, 20 µm. H) Recombinant X. laevis TOP2A possesses decatenating activity in vitro. Agarose gel of kinetoplast decatenation assay. Recombinant TOP2A promoted ATP-dependent decatenation of kinetoplast DNA.
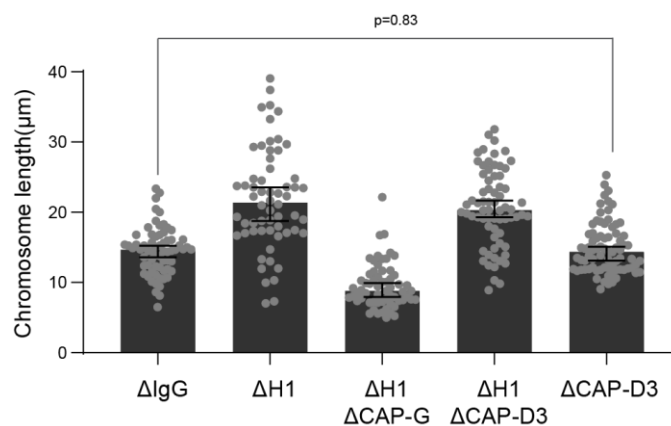

Figure S3. Condensin II depletion does not affect chromosome length (related to Figure 3)

Length of mitotic chromosomes in the indicated conditions after extract dilution showing no effect of CAP-D3 (condensin II) depletion in both mock and H1.8 depletion background. Each dot represents length of a single chromosome. Bars represent median +/- 95% C.I. The length of >50 chromosomes were measured in each condition for every experiment.

Choppakatla et al., Dec 2020-preprint copy- BioRxiv
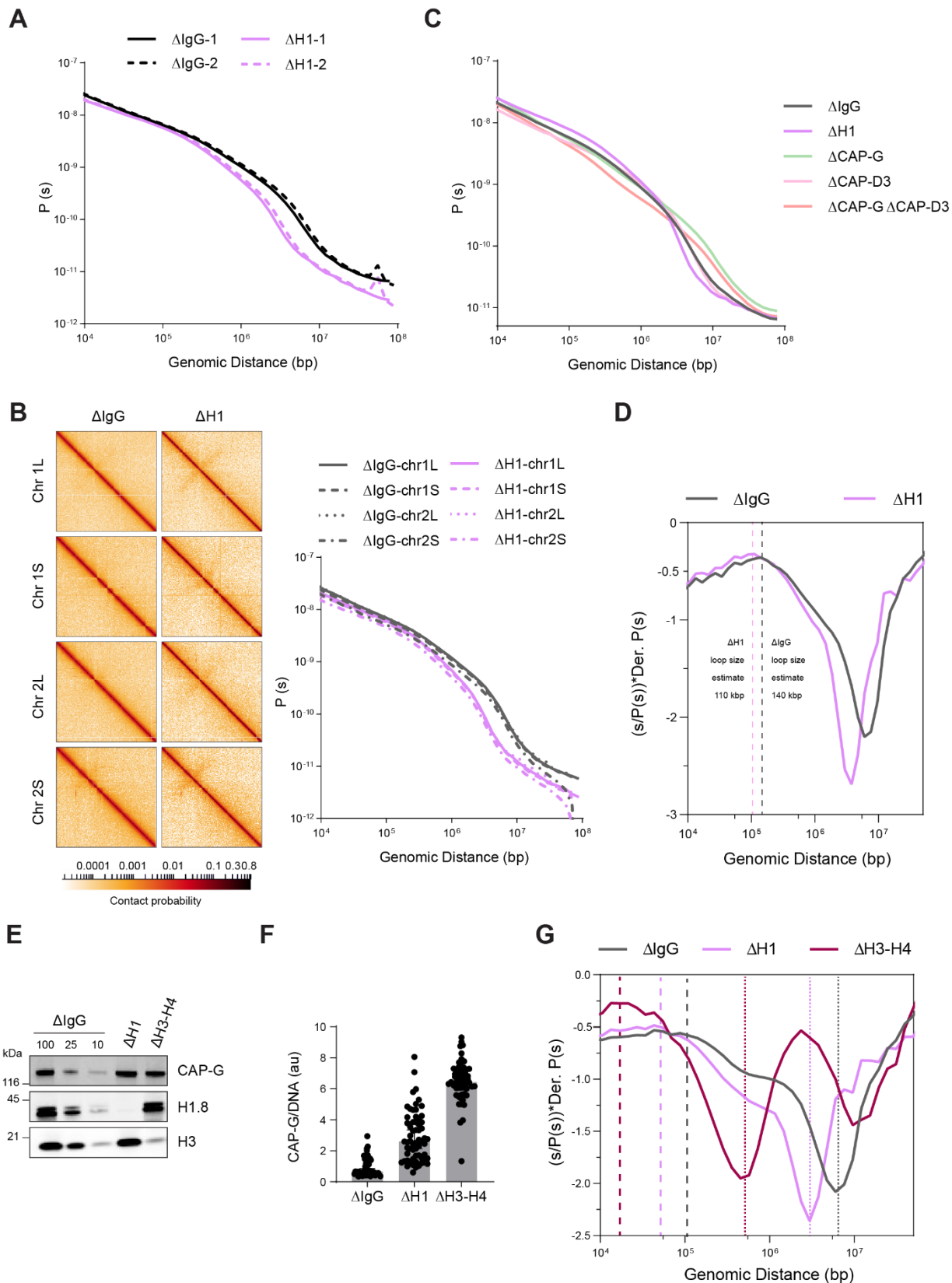
Figure S4. Effects of H1 and H3-H4 depletion on mitotic genome folding (related to Figure 4)

A) Contact probability decay curves of mitotic chromosomes in mock (ΔIgG) and H1-depleted (ΔH1) extracts from two different experiments showing the replicability of the Hi-C features. The solid and dashed lines are from biological replicates. B) Hi-C maps (left) binned to 500 kb, and contact probability curves (right) of single chromosomes showing the uniform effects of H1.8 depletion genome wide. C) Genome average contact probability decay curves upon H1.8, CAP-G and CAP-D3 depletions. D) Genome average contact probability derivative curves of dispersed metaphase chromosomes (as in **Figure 3A**) in mock (ΔIgG) and H1.8 depleted (ΔH1) extracts. The loop size estimates from the peak in the derivative plots are indicated. E) Western blotting showing the depletion of H3-H4 in extract using the H4K12ac antibody (Zierhut et al., 2014). F) Quantification of condensin I (CAP-G) immunofluorescence levels on chromosomes normalized to DNA in ΔH1 and ΔH3-H4 extracts. Each dot represents the average signal intensity of a single chromosome cluster (from one nucleus). Data plotted is median and 95 % C.I. >40 nuclei were quantified for each condition plotted. G) Hi-C probability decay derivative plots estimating the loop sizes in ΔH1 and ΔH3-H4 extracts. The dashed lines indicate the loop sizes in the corresponding conditions. The dotted lines indicate the layer sizes.
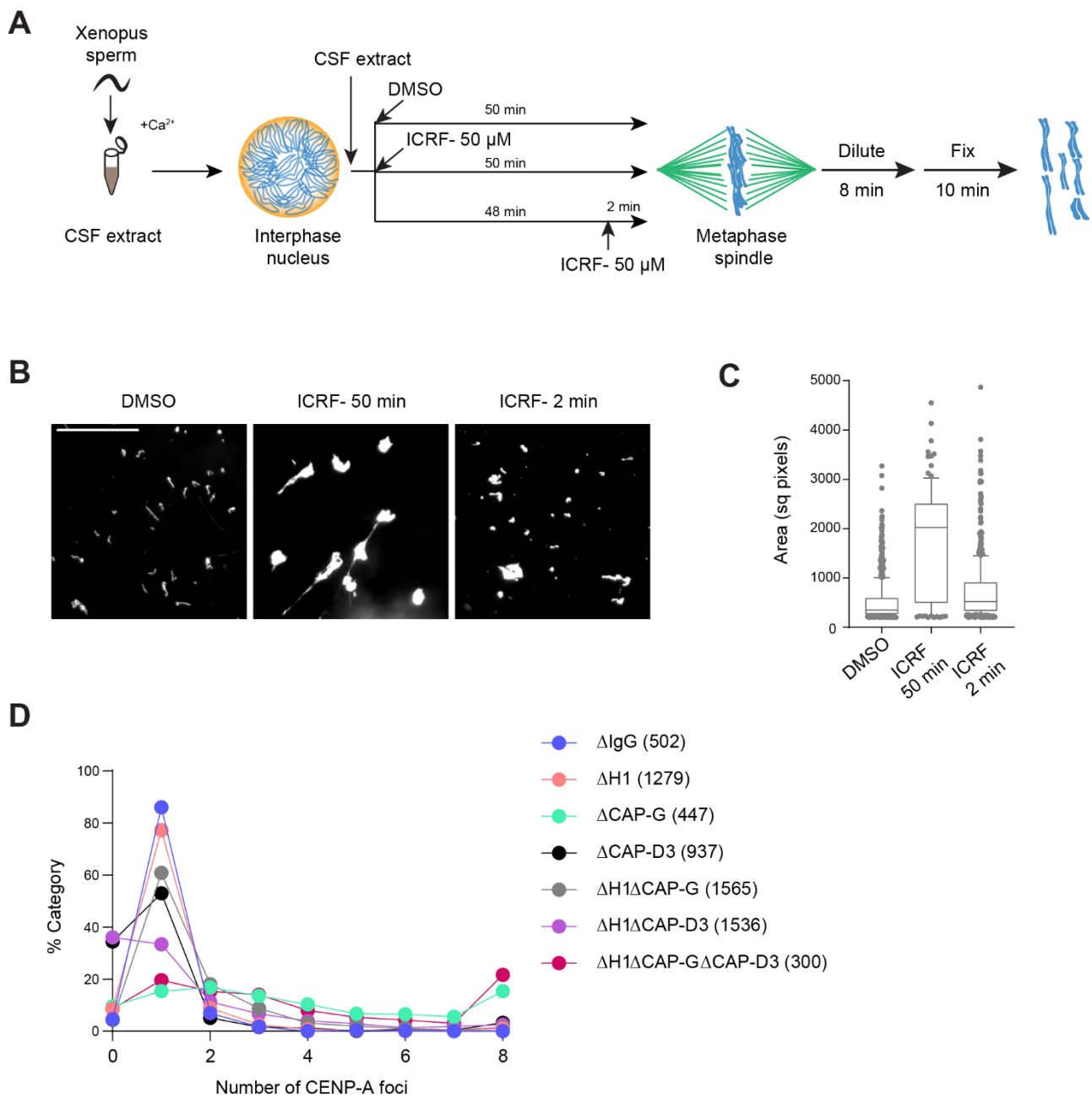
Figure S5. Regulation of chromosome individualization by topo II, condensins and H1.8 in *Xenopus* egg extracts (related to Figure 5)

A) Schematic of ICRF-193 addition to check for requirement of topo II activity in individualizing chromosomes. Interphase nuclei were first formed in ΔIgG or ΔH1 extracts, topo II inhibitor ICRF-193 (50 µM) was added to egg extracts, either together with corresponding depleted egg extracts and incubated for 50 min (ICRF-50 min), or 48 min after adding the depleted extracts, followed by 2 min incubation with ICRF-193 (ICRF-2 min). B) Metaphase extracts processed as A were diluted to disperse individualized chromosomes. Representative Hoechst images of chromosomes are shown. Bar, 20 µm. C) Quantification of the Hoechst-stained area of chromosomes in B. Each dot represents the area of a single chromosome or a chromosome cluster. Large values indicate the extent of chromosome clusters. The box shows the 10th-90th percentile limits of the sample values. >100 chromosomes or chromosome clusters were counted for each condition. D) Distribution of CENP-A foci per DNA mass in the experiment shown in **Figure 5A-C**. Clusters of unresolved chromosomes are represented by higher numbers (>2) of CENP-A foci per DNA mass indicates clusters. No detectable CENP-A focus in ΔCAP-D3 (Δcondensin II) extracts is due to low CENP-A signal, reflecting the reported role of condensin II in CENP-A loading (Bernad et al., 2011). The number noted in each sample label is the number of chromosomes/clusters counted in each condition.

Choppakatla et al., Dec 2020-preprint copy- BioRxiv
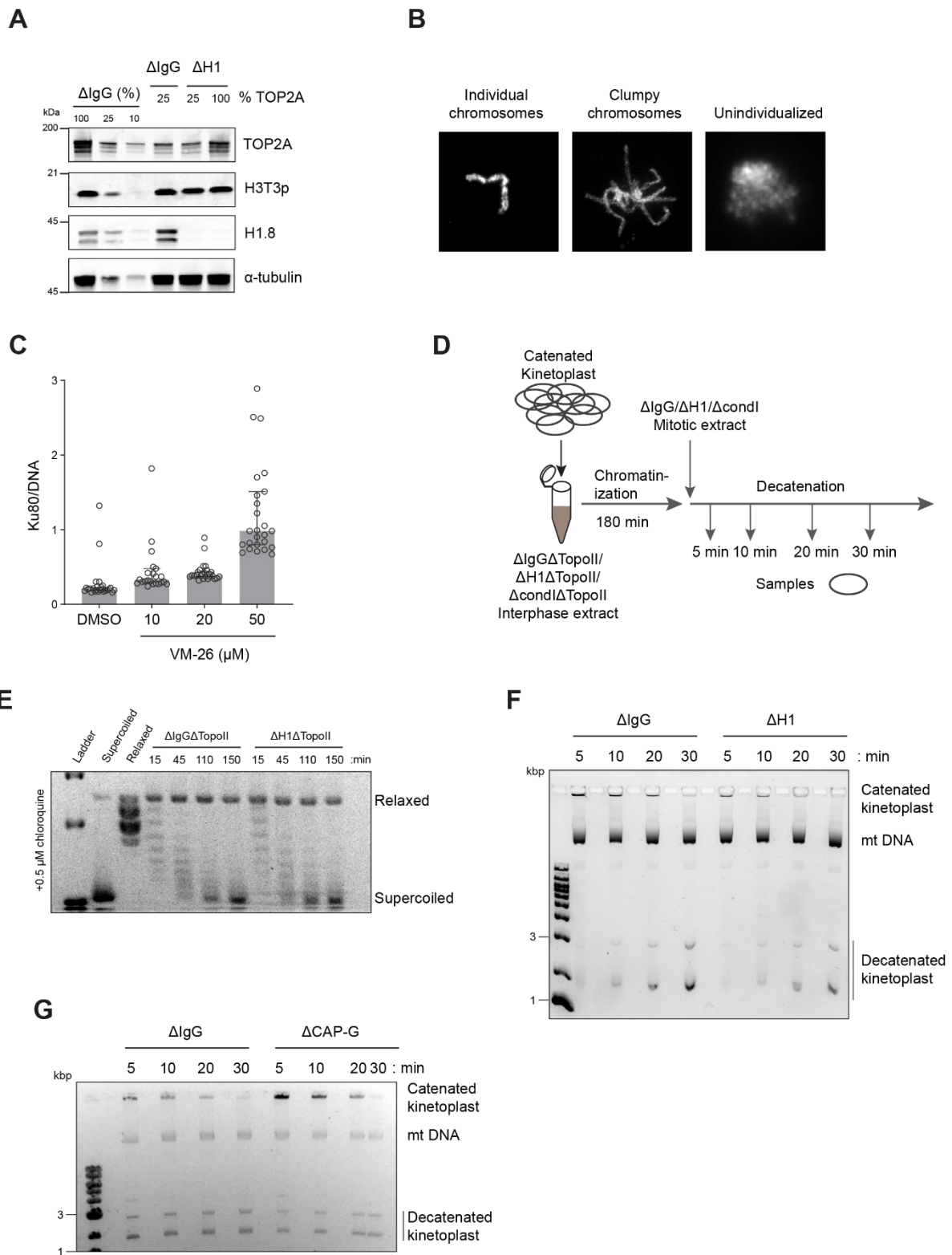
Figure S6. Topo II activity on mitotic chromosomes is stimulated by condensin I and suppressed by H1.8 (related to Figure 6)

A) Western blots showing partial depletion of TOP2A. Left three lanes; dilution series of total mock-depleted extracts (ΔIgG) for signal quantitation. Middle ΔIgG lane; extracts with 25% level of TOP2A. Right two ΔH1 lanes; extracts depleted of H1.8 with either 25% or 100% levels of TOP2A. B) Categories of chromosome clusters observed upon performing chromosome individualization assay. C) Quantification of Ku80 immunofluorescence signal levels on chromosomes normalized to Hoechst (DNA) signals. Extracts containing metaphase chromosomes were treated with increasing VM-26 concentration for 60 min. Each dot represents the average signal intensities of a single chromosome cluster from a nucleus. Bars represent median and 95% C.I. >25 chromosome clusters were counted per each time point. D) Experimental scheme for decatenation assay on chromatinized kinetoplast DNA. Catenated kinetoplast DNA was incubated with indicated ΔTOP2A interphase egg extract for 180 min to assemble nucleosomes without TOP2A. Mitosis was induced with adding corresponding metaphase extracts containing TOP2A. At indicated time after mitotic induction, DNA samples were recovered to monitor decatenation. E) Chromatinization time course on relaxed circular pBlueScript DNA showing no difference in chromatinization upon H1.8 depletion in interphase extract. Nucleosome formation introduces negative supercoils. F) Chromatinized kinetoplast decatenation time course showing no difference in kinetics of decatenation upon H1 depletion. G) Chromatinized kinetoplast decatenation time course showing no difference in kinetics of decatenation upon CAP-G depletion.